DETERMINATION OF THE SOURCE LOCATION OF THE 4.4 TO 5.2 MHz RADIATION OBSERVED BY THE *AMPTE IRM* SPACECRAFT

by

Andrew Edward Keller

A thesis submitted in partial fulfillment
of the requirements for the Master
of Science degree in Physics
in the Graduate College of
The University of Iowa

December 1990

Thesis supervisor: Professor Donald A. Gurnett

Graduate College
The University of Iowa
Iowa City, Iowa

CERTIFICATE OF APPROVAL

MASTER'S THESIS

This is to certify that the Master's thesis of

Andrew Edward Keller

has been approved by the Examining Committee for the thesis requirement for the Master of Science degree in Physics at the December 1990 graduation.

Thesis committee: _____
Thesis supervisor

_____
Member

_____
Member

Copyright by
ANDREW EDWARD KELLER
1990
All rights reserved

If it can't be expressed in figures, it is not science; it is opinion.
- from *Time Enough For Love*, by Robert A. Heinlein

ACKNOWLEDGMENTS

I would like to thank Dr. Gurnett and Dr. Roger Anderson for their essential help and criticism in assisting me in understanding what I was seeing, and Dr. Bruce Randall for his assistance in error analysis. I also would like to thank R. M. Alexander for her ideas and perspective, and Brent Studer for these TEX formats he sent to me; he got them from Tak Sakurai, who acquired them from Jim Leckband, *ad infinitum*. I expect to pass these on to other friends here; this compassionate spirit is truly a potent force and I both appreciate it and wish to see it grow here and everywhere. My thanks and love go to my parents and family, for they love and support me despite the facts that I walk on paths they do not fully understand and my steps are to a beat they do not hear. Finally, I thank all my friends, wherever they now live, for calling me "friend"; for without them, I would be a much poorer and sadder man. This research was largely funded by NASA research grant NAG5-1120.

ABSTRACT

Examination of the 4.4 to 5.2 MHz bands provided by the high-frequency electric receiver aboard the *AMPTE IRM* (*Active Magnetospheric Particle Tracer Explorers Ion Release Module*) shows the existence of an unusual narrow-band emission at a frequency of about 4.8 MHz. Initially, it was thought that this signal may be of natural origin. However, detailed examination shows that the signal turns on and off abruptly on time scales of seconds, suggesting that it is either spacecraft-generated interference or a human-made emission. High plasma densities generated by ion releases block out this signal, demonstrating that it is a real emission whose source is located somewhere outside of the *IRM*. Direction-finding measurements show that the radiation originates from the Earth. Lack of any coherent correlation in electric field strength versus radial distance plots suggest highly variable and/or multiple sources for this emission. Radiated power varied from 2.18 kW to as much as 4.33 MW, almost an order of magnitude greater than previously calculated. Suspected sources are over-the-horizon radars, pirate radio stations, or ionospheric heating experiments.

TABLE OF CONTENTS

Page

LIST OF TABLES vi

LIST OF FIGURES vii

CHAPTER

I. INTRODUCTION 1

II. THE *AMPTE IRM* SATELLITE 3

III. RADIATION FROM 4.4 TO 5.2 MHz 5

IV. DIRECTION-FINDING ANALYSIS 12

One-Dimensional Direction-Finding 12
Two-Dimensional Direction-Finding and the Problem of Background Noise 15
Estimation of Error in Direction-Finding Analysis 18

V. ELECTRIC FIELD STRENGTH ANALYSIS 22

Electric Field Strength versus Radial Distance 22
Power Analysis of the 4.8 MHz Radiation 23

VI. CONCLUSIONS 24

REFERENCES 26

APPENDIX I: TABLES 27

APPENDIX II: FIGURES 31

LIST OF TABLES

Table Page

1. Periods for which high-frequency electric field data from the *AMPTE IRM* spacecraft were available for this study. 28

2. Periods for which the data in the 4.8 MHz band of the high-frequency electric field receiver of the *AMPTE IRM* spacecraft showed a spin-correlated signal. 29

3. Average σ_Θ and σ_Φ values for each period that displayed a spin-correlated signal in the *AMPTE IRM* 4.8 MHz high-frequency electric field receiver band. 30

LIST OF FIGURES

Figure Page

1. Line drawing of the *AMPTE IRM* spacecraft 32

2. Spectrogram of the *AMPTE IRM* barium release on 27 December 1984. The range of the intensity scale runs from the instrument noise level (dark blue) to the receiver's saturation level (red). Note the plasma frequency cutoff by the cloud's electrons, and its effect on the band of interest, the intense, narrow band at the top of the spectrogram 34

3. Positions of the *IRM* spacecraft during the periods that high-frequency electric field data were taken. The Earth is the circle at the origin, and the Sun lies out of the plot, down the positive x-axis 36

4. Common logarithm of the electric field strength versus time on 8 June 1985 to demonstrate an instance where the signal suddenly disappears 38

5. Common logarithm of the electric field strength versus time on 5 March 1986 to demonstrate an instance where the signal abruptly appears 40

6. Polar (left) and rectangular plots of a simulated strong ($\sim$ 100 μV/m) source at $\Theta = 89.95°$, $\Phi = 65°$ (the solid line) with an omnidirectional background noise level of $\sim$ 2.4 μV/m (the dashed line). The open circles represent sample data points under this combined field. Note how the background noise fills the notches where the antenna alignment results in minimum reception 42

7. Polar (left) and rectangular plots of a simulated weak ($\sim$ 8.4 μV/m) source at $\Theta = 89.3°$, $\Phi = 65°$ (the solid line) with an omnidirectional background noise level of $\sim$ 2.4 μV/m (the dashed line). The open circles represent sample data points under this combined field. Note how the background noise fills the notches where the antenna alignment results in minimum reception 44

8. Polar (top) and rectangular plots of the 4.4, 4.8, and 5.2 (left to right) MHz bands for an arbitrary eight-minute period on 27 December 1984 where a spin-correlated signal was seen in the 4.8 MHz channel 46

9. Polar (top) and rectangular plots of the 4.4, 4.8, and 5.2 (left to right) MHz bands for an arbitrary eight-minute period on 21 April 1985 where a spin-correlated signal was seen in the 4.8 MHz channel 48

10. Polar (top) and rectangular plots of the 4.4, 4.8, and 5.2 (left to right) MHz bands for an arbitrary eight-minute period on 26 April 1985. On this day, no spin-correlated signal was seen in the 4.8 MHz band 50

11. Polar (top) and rectangular plots of the 4.4, 4.8, and 5.2 (left to right) MHz bands for an arbitrary eight-minute period on 8 June 1985 where a spin-correlated signal was seen in the 4.8 MHz channel 52

12. Polar (top) and rectangular plots of the 4.4, 4.8, and 5.2 (left to right) MHz bands for an arbitrary eight-minute period on 9 June 1985 where a spin-correlated signal was seen in the 4.8 MHz channel 54

13. Polar (top) and rectangular plots of the 4.4, 4.8, and 5.2 (left to right) MHz bands for an arbitrary eight-minute period on 5 March 1986 where a spin-correlated signal was seen in the 4.8 MHz channel 56

14. Direction of the source of the spin-correlated 4.8 MHz data in the *IRM*'s spin plane on 27 December 1984. The projection of the Earth in this plane is denoted by the circle drawn, the projection of the spacecraft's course is the jagged line indicated, and the source directions are the dotted lines running between them 58

15. Direction of the source of the spin-correlated 4.8 MHz data in the *IRM*'s spin plane on 21 April 1985. The projection of the Earth in this plane is denoted by the circle drawn, the projection of the spacecraft's course is the jagged line indicated, and the source directions are the dotted lines running between them 60

16. Direction of the source of the spin-correlated 4.8 MHz data in the *IRM*'s spin plane on 8 June 1985. The projection of the Earth in this plane is denoted by the circle drawn, the projection of the spacecraft's course is the jagged line indicated, and the source directions are the dotted lines running between them 62

17. Direction of the source of the spin-correlated 4.8 MHz data in the *IRM*'s spin plane on 9 June 1985. The projection of the Earth in this plane is denoted by the circle drawn, the projection of the spacecraft's course is the jagged line indicated, and the source directions are the dotted lines running between them 64

18. Direction of the source of the spin-correlated 4.8 MHz data in the *IRM*'s spin plane on 4-5 March 1986. The projection of the Earth in this plane is denoted by the circle drawn, the projection of the spacecraft's course is the jagged line indicated, and the source directions are the dotted lines running between them 66

19. Direction of the source of the 454 and 504 kHz Auroral Kilometric Radiation data in the *IRM*'s spin plane on 27 December 1984. The projection of the Earth in this plane is denoted by the circle drawn, the projection of the spacecraft's course is the jagged line indicated, and the source directions are the dotted lines running between them 68

20. Direction of the source of the 302 kHz Auroral Kilometric Radiation data in the *IRM*'s spin plane on 4 March 1986. The projection of the Earth in this plane is denoted by the circle drawn, the projection of the spacecraft's course is the jagged line indicated, and the source directions are the dotted lines running between them . . 70

21. Graphic display of possible source directions. The plane of the page is the source plane: perpendicular to the spin plane and along the Φ direction. Θ, the out-of-spin-plane source angle, determines the four rays a free source may lie along, indicated by the circled points. Presence of background noise implies the arc between the points on one side of the spin axis or the other. Triangulation determines which pair of points is meaningful 72

22. This set of 3 plots display the source arcs of the 4.8 MHz signal as seen from the *IRM* on 27 December 1984. The Earth, as seen from the spacecraft, is the circle and is scaled to its apparent size; the Sun's position is indicated by the point labelled; and the source positions are the vertical segments. This figure indicates a source somewhat in front of the Earth 74

23. This set of 4 plots display the source arcs of the 4.8 MHz signal as seen from the *IRM* on 21 April 1985. The Earth, as seen from the spacecraft, is the circle and is scaled to its apparent size; the Sun's position is indicated by the point labelled; and the source positions are the vertical segments. This figure indicates a source somewhere on the Earth 76

24. This set of 5 plots display the source arcs of the 4.8 MHz signal as seen from the *IRM* on 8 June 1985. The Earth, as seen from the spacecraft, is the circle and is scaled to its apparent size; the Sun's position is indicated by the point labelled; and the source positions are the vertical segments. This figure indicates a source somewhere on the Earth 78

25. This plot displays the source arcs of the 4.8 MHz signal as seen from the *IRM* on 9 June 1985. The Earth, as seen from the spacecraft, is the circle and is scaled to its apparent size; the Sun's position is indicated by the point labelled; and the source positions are the vertical segments. This figure indicates a source somewhere on the Earth 80

26. This set of 5 plots display the source arcs of the 4.8 MHz signal as seen from the *IRM* on 4-5 March 1986. The Earth, as seen from the spacecraft, is the circle and is scaled to its apparent size; the Sun's position is indicated by the point labelled; and the source positions are the vertical segments. This figure indicates a source somewhat in front of the Earth 82

27. This set of 2 plots display the source arcs of the 454 and 504 kHz AKR as seen from the *IRM* on 27 December 1984. The Earth, as seen from the spacecraft, is the circle and is scaled to its apparent size; the Sun's position is indicated by the point labelled; and the source positions are the vertical segments. This figure indicates a source somewhat in front of the Earth, just like the 4.8 MHz signal 84

28. This set of 5 plots display the source arcs of the 302 kHz AKR as seen from the *IRM* on 4 March 1986. The Earth, as seen from the spacecraft, is the circle and is scaled to its apparent size; the Sun's position is indicated by the point labelled; and the source positions are the vertical segments. This figure indicates a source somewhere near the Earth 86

29. Graph of calculated electric field strength versus distance from the Earth for all measurements taken, with error bars. A least-squares fit has been applied, and the resulting slope and correlation coefficient noted (a coefficient of 1.0 means a perfect fit) 88

30. Graph of calculated electric field strength versus distance from the Earth for each separate continuous receiving period, with error bars. A least-squares fit has been applied to each, and the resulting slope and correlation coefficient noted (a coefficient of 1.0 means a perfect fit) 90

CHAPTER I

INTRODUCTION

Many spacecraft have explored the low frequency electromagnetic waves present in the neighborhood of the Earth; that is, frequencies up to $\sim$ 1 MHz. Higher radio frequencies in the MHz range had not been well examined until 1984, when the *Active Magnetospheric Particle Tracer Explorers* were launched. *AMPTE*'s *Ion Release Module* or *IRM* carried an electric field receiver capable of measuring frequencies up to 5.6 MHz. The only other spacecraft presently capable of observing such high frequencies is the *Galileo* probe now on its way to Jupiter, and the *ISEE-3* or *ICE* spacecraft, which is also now in interplanetary space away from the Earth.

Once the *IRM* was placed in orbit, the spacecraft detected strong electric field signals in its 4.8 MHz channel. In an attempt to determine the cause of these signals, we considered four major types of sources:

1) the source is some form of spacecraft interference,

2) the source is some kind of radiation of extraterrestrial origin,

3) the source is some natural radiation of terrestrial origin, or

4) the source is some human-made radiation of terrestrial origin.

If the source of this radiation turned out to be natural radiation from the Earth, then this radiation would be of considerable scientific interest. Therefore, we decided to investigate the origin of this signal. While we were carrying out

the prerliminary investigation, LaBelle *et al.* [1989] published a paper devoted to an overview of the data collected by the *IRM* in the electric field receiver's MHz frequency channels. In that paper, they stated that they believed that these signals were caused by an Earth-based, human-made source, and suggested that terrestrial over-the-horizon radars might be the specific cause of the emission seen in the 4.8 MHz band. However, their belief is based only on a calculation of power received by the *IRM* and includes no direction-finding to identify the source location. The purpose of this thesis was to do this direction-finding, to examine the dependence of the electric field strength on distance, and to corroborate Labelle's power calculation of the 4.8 MHz emission in order to conclusively establish, if possible, the location and nature of the source responsible for this signal.

CHAPTER II

THE *AMPTE IRM* SATELLITE

The *Active Magnetospheric Particle Tracer Explorers* (*AMPTE*) project was an international collaboration to explore both the Earth's magnetosphere and to observe the effects of the environment on lithium and barium clouds released along its orbit. The *AMPTE* mission consisted of three spacecraft launched in August of 1984: the *United Kingdom Satellite* or *UKS* (Great Britain), the *Charge Composition Explorer* or *CCE* (United States), and the *Ion Release Module* or *IRM* (West Germany). The data used in this thesis came from the *IRM* spacecraft, which is shown in Figure 1. The *IRM* carried a forty-two step high-frequency electric receiver that was constructed at the University of Iowa. This receiver provided spectrum measurements ranging from 100.8 kHz to 5.6 MHz, and was capable of obtaining a complete set of measurements from all of its channels every 2 seconds [Häusler, *et al.*]. The bandwidth of each channel in the receiver was 10 kHz. The receiver was connected to a 47.42 meter ($\sim$ 140 foot) tip-to-tip electric dipole antenna mounted on the spacecraft's body. Since the *IRM* was spin-stabilized with a period of $\sim$ 4.5 seconds and the antenna was oriented perpendicular to the spin axis, the antenna rotated in a plane perpendicular to the spin axis. The spin axis was oriented initially at $-22.8°$ Declination and $6^{h}\ 39^{m}$ Right Ascension. This orientation was modified somewhat during subsequent ion releases. The *IRM* had a

highly elliptical orbit, varying from a perigee altitude of 557 km to an apogee radial distance of 18.83 Earth radii. The orbital period was 44.3 hours, and the orbital plane was inclined 28.6° to the equatorial plane.

CHAPTER III

RADIATION FROM 4.4 TO 5.2 MHz

Figure 2 shows a frequency-time spectrogram of a barium release on 27 December 1984. The time is on the abscissa and the frequency measured is on the ordinate. The electric field strength at a particlar time and frequency is given by a color at that point, with blue being the lowest intensity, and red being the highest.

The spectrum shows the effect of a barium cloud. Prior to the barium release, the electric field intensities are as shown on the extreme left of Fig. 2. The broad red and yellow emissions between 100 kHz and 1 MHz are due to Auroral Kilometric Radiation, also known as AKR. AKR is a very sporadic, intense radio emission produced in the auroral regions of the Earth. Above 1 MHz, galactic radio emission can be seen as the light blue region just around a narrow-band emission from 4.4 to 5.2 MHz near the top of the spectrogram. Similar narrow-band emissions of comparable intensity were found in the 4.4 to 5.2 MHz region on other days, and are the topic of this thesis. The barium cloud was created by releasing a canister containing barium from the *IRM* and exploding it about 1 kilometer from the spacecraft. The resulting cloud of neutral barium was quickly ionized by solar radiation, thereby producing a dense, expanding cloud of plasma that enveloped the *IRM* a few seconds after the explosion. When the cloud enveloped the spacecraft at about 1232 UT, the electrons blocked external radiation at frequencies below

the electron plasma frequency $f_{pe} = 9000\sqrt{n_e}$ Hz, where n_e is the electron number density in cm^{-3}. The frequency f_{pe} is indicated by the propagation cutoff marked on the spectrogram. Note that the propagation cutoff affects the narrow-band emission in the 4.4 to 5.2 MHz range, the galactic radiation, and the AKR equally, implying that the narrow-band emission is a propagating signal that originates from outside the *IRM* itself.

High-frequency data from six time periods were studied: in 1984, 27 December; in 1985, 21 and 26 April and 8 and 9 June; and in 1986, 4 and 5 March in a single period crossing midnight. The exact intervals during which data was recorded are shown in Table 1. Figure 3 depicts the spacecraft's position in relation to the Earth during the intervals examined. The x- and y-axis are in Geocentric Solar Ecliptic coordinates; thus, the positive x-axis points to the Sun. The electric field signal transmitted to the ground by the spacecraft data system was expressed in terms of the common logarithm of the antenna voltage in the channel in microvolts (μV). Plotting the logarithm of the antenna voltage against time showed that a spin-correlated emission usually, but not always, existed in the 4.8 MHz channel of the receiver. Examples of spin-correlated emission can be seen in Figure 4 prior to the emission's disappearance and in Figure 5 after its reappearance. These figures plot the electric field strength versus time and demonstrate that the emission can abruptly appear or disappear. During times in which the emission is present, the amplitude exceeds 10 μV/m (and, at times, 100 μV/m), and exhibits relatively deep drops about every 20 seconds or so. These drops indicate spin-correlation despite the 20 second interval. If the 4.8 MHz channel were continuously monitored, one

would expect emission drops every half of a spin period ($\sim$ 2.2 sec). This instrument, however, only measures the 4.8 MHz channel once every 2 seconds, and so is usually *not* measuring when a emission drop would occur. Measurement of the drop only happens when the emission drop is present during a measurement, and this works out to be at about 20 second intervals.

Table 2 shows times in which a spin-correlated emission exists in the 4.8 MHz channel. It is interesting to note the differences in Tables 1 and 2. The source of the emission seems to appear and disappear in no set pattern; and, as noted before, the emission can turn on and off suddenly (Figs. 4 and 5). Figure 4 shows the emission abruptly disappearing at 2204:37 UT, while in Figure 5, the emission suddenly reappears at 0309:24 UT. Because human-made sources are much more likely to turn on or off in this manner, these observations strongly suggest a human-made cause for the emission.

A spinning dipole antenna provides a way to investigate the directional nature of incoming radiation. Since the electric field of a radio wave is perpendicular to its direction of propagation, the maximum antenna voltage will occur when the antenna is perpendicular to the source direction; conversely, the minimum antenna voltage will occur when the antenna is most nearly parallel to the source direction. The source direction is then in a plane perpendicular to the antenna orientation at the time of maximum antenna voltage.

Because the antenna rotates, the logarithm of the electric field strength detected by the *IRM* can be plotted against the antenna angle with respect to the Sun (instead of time, as in Figs. 4 and 5) in either a polar or a rectangular graph.

In the process of studying the polar and rectangular graphs of electric field strength versus antenna angle, it was discovered that an omnidirectional background "noise" level existed, below which no spin-correlated emission could be detected. To understand what effect a background noise level had on a localized source of radiation, it was instructive to simulate spin-correlation measurements in the presence of such a background noise level.

The effect of a background noise level of ~ 2.4 μV/m on the field of a localized radiation source is simulated in Figures 6 and 7, and is expressed both in a polar (left) and a rectangular (right) plot in each figure. The curve with the sharply pointed nulls is the radiation source alone on both polar and rectangular plots, while the dashed circle (polar plot) or line (rectangular plot) is the omnidirectional background noise. The small, open circles represent simulated data points measured in such an electric field arrangement with a random $\pm 10\%$ variability to simulate measurement fluctuations. The concentric, solid line circles in the polar plots are contours of electric field strength. The innermost of the concentric circles is the contour of 1 μV/m. The next circle is the contour of 10 μV/m, the third circle is the contour of 100 μV/m, and the outermost circle is the contour of 1 mV/m. The background noise level has an effect on the spin-correlation analysis, because the minima of the spin-correlated emission will be lost below the background noise, causing the true value of the null in the radiation to disappear, even for a strong source. In the rectangular plot of Figure 6, note that over an order of magnitude is obscured by the background noise (from the null point up to the dotted line). Since the magnitude of the source's out-of-plane angle (Θ) is inversely proportional

to the depth of the null compared to the peak height, reduction of the null depth by background noise will increase the apparent out-of-plane angle. If the source is weaker or farther away, this background noise will not only enhance the out-of-plane angle by reducing the difference between the peak and null values, but will also change the shape of the distribution of the data points (Fig. 7, right panel). It is a common practice to determine the source direction from the direction of the spin-correlation null; but because the background noise can obscure the depth of the null, we added 90° to each antenna angle we measured. This placed the peak of the spin-correlation along the source direction. The main advantage of this "90° offset" procedure is that as long as the peak electric field strength is above the background, it is possible to find the source direction from simple visual inspection. The offset procedure was carried out in Figures 6 and 7, and the source direction is indicated by the dotted lines in the polar and rectangular graphs. The spin-plane source angle, Φ, is measured counterclockwise from the upward vertical axis to the dotted line in the polar plots of Figs. 6 and 7.

Figures 8 through 13 show the directionality of the emission for a subset of data on each observing day for the 4.4, 4.8, and 5.2 MHz channels (except 26 April 1985, where the lack of emission is demonstrated). A polar plot of each channel is shown in the upper half of each figure: the Sunward direction is always the upward vertical axis, and the concentric circles here have exactly the same values as the concentric circles in Figures 6 and 7. The lower half of each figure is a rectangular plot of the electric field strength versus the polar angle ϕ_{IRM} at which the sample was obtained in spacecraft coordinates: the spin axis is the positive z-axis, and the

angle is measured from the positive x-axis, which points in the Sunward direction. From left to right, the channels are: 4.4 MHz, 4.8 MHz, 5.2 MHz. These three frequencies are consecutive channels in the high-frequency receiver.

The 4.4 and 5.2 MHz channels were interesting only in that when spin correlation was present in either channel, its direction was always the same as that of the 4.8 MHz channel. The spin correlations of these channels were never very strong; that is, the peaks in electric field strength were never very far above the background level, with the exception of a period of 100 minutes on 8 June 1985 in the 5.2 MHz channel. Even in this case, the peak electric field strength was an order of magnitude smaller than the neighboring 4.8 MHz channel. These emissions were also generally short-lived compared to the 4.8 MHz emission, usually dying down to background in much less time than the Day 159, 1985, 5.2 MHz emission mentioned above. As a result, much more time and effort was spent analyzing the 4.8 MHz emissions.

Figure 8 displays the electric field strengths for the period 1150:01 to 1157:59 UT on 27 December 1984. Note in the 4.4 MHz polar graph (upper left) that the points are grouped together at particular angles with gaps between them. This "spotted pattern," which can be easily seen in both the 4.4 and 5.2 MHz plots, is a numerical "beat frequency" effect between the spacecraft rotation rate and the sampling rate of the antenna voltage. The 4.8 MHz channel demonstrates that the spin-correlated electric field does indicate a source direction (the definite humps in the rectangular plot). The electric field strength here is rather weak, as can be seen by the similarity of the 4.8 MHz polar and rectangular plots to those in Figure 7.

The period from 0110:01 to 0117:59 UT on 21 April 1985 is displayed in Figure 9. In contrast to the spotted pattern in Figure 8, the 4.4 and 5.2 MHz plots show a smooth distribution over angle. The 4.8 MHz emission here is strong (note the strong similarity of the 4.8 MHz plots to those of Figure 6). Figure 10 shows electric field strengths from 26 April 1985 over the period 0620:01 to 0627:59 UT. Note the total *lack* of spin-correlated emission in the 4.8 MHz channel, as this was the norm for the whole observation period on that day.

Figure 11 displays a strong 4.8 MHz emission on 8 June 1985 from 1840:00 to 1847:58 UT, during the second interval of the emission's presence that day. Figure 12, made from 9 June 1985, 1712:00 to 1719:58 UT data, show a moderately strong 4.8 MHz emission, and a slight directionality in the 5.2 MHz channel that matches the direction of the 4.8 MHz emission. The electric field strengths from 0312:00 to 0319:58 UT on 5 March 1986 are displayed in Figure 13. On this day, the angular values again made a spotted pattern, again due to the spin rate being just the right value to cause the "beat frequency" phenomenon. The 4.8 MHz emission is again strong, but no spin-correlation is present in either the 4.4 or 5.2 MHz channels.

Once these observations were obtained, the next logical step was to determine the direction of arrival in order to determine the source position.

CHAPTER IV

DIRECTION-FINDING ANALYSIS

The position of the *IRM* and the orientation of the spacecraft's spin axis, both in Geocentric Solar Ecliptic coordinates, was provided on the spacecraft data record along with the high-frequency electric receiver information. Since the source of the emission is outside the spacecraft, it should be possible to combine the information about the *IRM*'s position and coordinate system with the calculated source direction to determine the location of the emission.

One – Dimensional Direction – Finding

Theoretically, a dipole antenna in the radiation field of a localized source should detect an electric field strength with the following dependence:

$$E^2 = A_0 + A_1 \cos^2(\varpi - \Phi), \text{ where} \tag{1}$$

E = the detected electric field strength,

ϖ = the angle from the Sun,

Φ = the value of ϕ_{IRM} in the direction of peak electric field,

A_0 = constant, and

A_1 = constant.

This equation is essentially the same as that used by Kurth *et al.* [1975] in doing a similar direction-finding study on Auroral Kilometric Radiation.

Now, Equation 1 can be manipulated into the form

$$E^2 = C_1 + C_2 \cos 2\varpi + C_3 \sin 2\varpi,$$

and the constants C_1, C_2, and C_3 can be found from the minimization of the function

$$\chi^2 = \sum_i \left[E_i^2 - C_1 - C_2 \cos 2\varpi_i - C_3 \sin 2\varpi_i\right]^2,$$

where

E_i = the electric field strength at data point i, and

ϖ_i = the ϕ_{IRM} value at data point i.

The minimization is accomplished through evaluation of $\frac{\partial \chi^2}{\partial C_k} = 0$ for each k; that is,

$$\sum_i \begin{bmatrix} E_i^2 \\ E_i^2 \cos 2\varpi_i \\ E_i^2 \sin 2\varpi_i \end{bmatrix} = \sum_i \begin{bmatrix} 1 & \cos 2\varpi_i & \sin 2\varpi_i \\ \cos 2\varpi_i & \cos^2 2\varpi_i & \sin 2\varpi_i \cos 2\varpi_i \\ \sin 2\varpi_i & \cos 2\varpi_i \sin 2\varpi_i & \sin^2 2\varpi_i \end{bmatrix} \begin{bmatrix} C_1 \\ C_2 \\ C_3 \end{bmatrix}. \quad (2)$$

To fit Equation 1 to the observed electric field strengths, the intervals of spin-correlated emission were broken up into eight-minute segments. Since successive measurements were about 2 seconds apart and the spin period varied between 4.375

sec to 4.471 sec, each measurement is about half a rotation from the previous point. Thus, a large number of points is required to obtain a good sampling over the full range of ϕ_{IRM}. Since only C_2 and C_3 are required to determine Φ, we can now determine whether the direction of arrival corresponds to the projection of the Earth in the spacecraft spin plane.

In Figures 14 through 20, the Earth was projected onto the spin plane of the *IRM* using the spacecraft's position information. This projection is represented by the circle at the origin. The source plane directions, determined by the value of Φ calculated by the fitting program, are drawn as dotted lines on these figures. On some of these figures, a jagged line is visible at the end of the dotted lines away from the Earth. This is the *IRM*'s trajectory projected onto the spin plane. The jagged line is not very visible on Figures 14, 17, and 19 because the orbit section is so short that the jagged line of the orbit is obscured by the dotted lines indicating the source direction.

Figure 14 indicates a location somewhat in front of the Earth, and it also shows the largest spread of Φ values of any of these figures. This large spread can be attributed to the weak electric field strength observed during this period (see Fig. 8). The small difference between the peak and the null/background electric field strength contributes significantly to the error in the source direction calculated from the plots on this day. During this period, the electric field was so weak that for a period of $\sim$ 35 minutes the source direction turned to within 30° of the Sun. To confirm the direction determination of the fitting program, 454 and 504 kHz AKR data, gathered through the *IRM*'s high-frequency receiver, was also analyzed

by the program for this same period. The result of the fitting program's analysis of the AKR data is shown in Figure 19. This radiation was not strong and it did not point to the Earth either, but it does point toward the same region of space as the 4.8 MHz band.

In the cases of Figures 15, 16, and 17, the Φ direction is always toward the Earth, with an apparent tendency to favor the anti-Sunward side. The presence of two separated orbit sections in Figure 16 reflects the disappearance of the emission in the intervening time. Figure 18 also has a missing orbit section because the emission disappeared over an interval on this day as well. The direction of the source on 4-5 March 1986 indicates a source somewhat in front of the Earth, much like 27 December 1984. Thus, an AKR analysis was done for 4 March, similar to that done for 27 December 1984. The result, shown in Figure 20, shows that the AKR originates from the Earth, leaving a 10°–15° discrepancy between the AKR direction and the 4.8 MHz emission's direction.

By this analysis, then, the 4.8 MHz emission seems to originate from the Earth, but it does not completely explain the deviations from the Earth found on 27 December 1984 or 4-5 March 1986.

Two – Dimensional Direction – Finding and the Problem of Background Noise

The source direction in the spin plane, Φ, is not the only piece of information obtainable from rectangular plots like those in Figures 8-13. If the electric field peaks with a value E_0, then the detected electric field null has a value $E_0 \cos\Theta$, where Θ is the θ_{IRM} value of the source determined by the fitting program. (θ_{IRM}

is the out-of-spin-plane angle in the spacecraft's coordinate system, measured from the spin axis.) If this were the only emission present, one would expect to find the source along one of the four directions indicated by the circled points on Fig. 21. This is a display of the out-of-spin-plane angle value Θ of a localized source in the source plane. However, if some background noise is present, there is no way to conclusively determine whether the circled points show the true source directions or are merely distorted values caused by the background noise. The amount of background noise in any given data set is unknown; nor is it known how this background noise is produced. The background noise may be due to spacecraft interference, and this interference may change from place to place around the Earth. Even if the background noise were removed, the noise could be orders of magnitude larger than the null values, losing the true Θ value irretrievably. Therefore, because of the background noise, one cannot be certain of just how far off the spin plane the source is; what Θ *does* indicate is that the source cannot be any farther from the spin plane than $90° - \Theta$ above or below that plane, though it could be anywhere in the wedge $90° - \Theta \leq \Theta_{true} \leq 180° - \Theta$ (the arc shown in Fig. 21).

For the Earth to be the source, then, it is necessary to show that the Earth always appears somewhere in the wedge dictated by the calculation of Θ. Recall Equation 1:

$$E^2 = A_0 + A_1 \cos^2(\varpi - \Phi), \text{ or} \tag{1}$$

$$E^2 = C_1 + C_2 \cos 2\varpi + C_3 \sin 2\varpi.$$

The minimum electric field gives the condition $A_0 = E_0^2 \cos^2 \Theta$, and the max-

imum field yields $A_1 = E_0^2 \sin^2 \Theta$. Expressing A_0 and A_1 in terms of C_1, C_2, and C_3 is a simple matter of algebra, so with the C_k evaluated by the fitting program, Θ can be calculated, and the resulting source wedge can be plotted to determine if the Earth always falls within the wedge.

Each of the Figures 22 through 28 is an azimuthal projection of the source wedges in the spacecraft's coordinate system. The important landmarks in these plots are the Sun (indicated by the small circle near the word "Sun"), the Earth (the larger circle), and the computed source wedges (the vertical line segments). As the *IRM*'s spin axis was always oriented within 45° of the Geocentric Solar Ecliptic South pole, the Earth's North pole appears on the lower half of the Earth. The Earth's circle has been appropriately scaled to reflect its apparent size from the spacecraft, and as the spacecraft moved, the Earth's position and size as seen from the *IRM* changed; and every time the Earth changed angular position, a new plot was made reflecting the changes. These changes display the time evolution of the source direction. If no background noise existed, only the endpoints of the line segments would need to be considered to determine if the Earth was the source; but since a background noise level is unknown, the Earth must fall somewhere along the source wedge.

Figure 22 displays the source wedges of the 4.8 MHz emission seen on 27 December 1984. Here it can be seen that despite the tendency for the direction to lead the Earth, the out of plane angle seems to show that the North pole of the Earth is favored as a source. Figure 27 shows that the AKR directions had a similar tendency to lead the Earth as well. Figure 23 shows the source of this emission is

associated with the Earth while expressing a variablility in position of about 8°. The effect of backgound noise is very apparent in these plots. The source wedges are expanded to at least 15° above and below the Earth.

Figure 24 most clearly shows that the emission must originate at the Earth. While the Earth during this period moves considerably from the *IRM*'s viewpoint, the source direction consistently points to the Earth throughout the observation period, which is broken into two parts by the disappearance of the emission between 1500 and 1546 UT. The following day's two source wedges are shown in Figure 25, and again the Earth is well bracketed by the direction-finding measurements. Again, background noise spreads the wedge $\sim$ 15° above and below the Earth.

The data for 4-5 March 1986 is also broken into two segments by the emission's 118 minute disappearance soon after midnight. In this case, the direction of arrival tends toward the Sunward side of the Earth by as much as $\sim$ 10°. The Auroral Kilometric Radiation at 302 kHz always originated from the Earth (see Fig. 28). Background noise is again responsible for the extension of the line segments.

Thus, the two-dimensional direction-finding strongly supports the idea that the 4.8 MHz emission originates at the Earth. However, a determination of the magnitude of the errors inherent in the calculation of both Θ and Φ may help reveal how the discrepancies of 27 December 1984 and 4-5 March 1986 can be understood.

Estimation of Error in Direction – Finding Analysis

The errors in measurement can be classified as either systematic or statistical errors. In this section, we will be concerned primarily, but not exclusively, with statistical errors.

One of these systematic errors for the source wedge positions is the precision of the reported *IRM* position. The altitude coordinate was given to the nearest degree, while the azimuthal position was noted in local time to the nearest tenth of an hour. Thus, in addition to uncertainties associated with the calculated quantities, the source arcs may be off by $\pm 1.5°$ in the Ecliptic plane, and by $\pm 1°$ perpendicular to the Ecliptic plane. We next consider the statistical errors associated with the calculated quantities, but before discussing the statistical error values in the calculated variables E_0, Θ, and Φ, we will discuss our method of obtaining them. Recall again Equation 1:

$$E^2 = A_0 + A_1 \cos^2(\varpi - \Phi), \text{ or} \tag{1}$$

$$E^2 = C_1 + C_2 \cos 2\varpi + C_3 \sin 2\varpi.$$

In a fashion similar to the method of obtaining the values C_1, C_2, and C_3, the errors in these values, σ_{C_1}, σ_{C_2}, and σ_{C_3}, were calculated by considering the next term in a Taylor expansion of χ^2 around the minimum value χ_0^2:

$$\chi^2 = \chi_0^2 + \sum_k \left(\frac{\partial \chi_0^2}{\partial C_k} \delta_{C_k} \right) + \sum_{j,k} \left(\frac{\partial^2 \chi_0^2}{\partial C_j \partial C_k} \delta_{C_j} \delta_{C_k} \right) + \ldots$$

In computational terms, this leads to the evaluation of each δ_{C_k} in an equation which bears a strong resemblance to Equation 2:

$$\sum_i \begin{bmatrix} \Delta E_i^2 \\ (\Delta E_i^2)\cos 2\varpi_i \\ (\Delta E_i^2)\sin 2\varpi_i \end{bmatrix} = \sum_i \begin{bmatrix} 1 & \cos 2\varpi_i & \sin 2\varpi_i \\ \cos 2\varpi_i & \cos^2 2\varpi_i & \sin 2\varpi_i \cos 2\varpi_i \\ \sin 2\varpi_i & \cos 2\varpi_i \sin 2\varpi_i & \sin^2 2\varpi_i \end{bmatrix} \begin{bmatrix} \delta_{C_1} \\ \delta_{C_2} \\ \delta_{C_3} \end{bmatrix}$$

where

$$\Delta E_i^2 = E_i^2 - C_1 - C_2 \cos 2\varpi_i - C_3 \sin 2\varpi_i,$$

$$\delta_{C_k} = \sqrt{n} \cdot \sigma_{C_k},$$

n = the number of data points in a set, usually 240,

and the values previously found for C_1, C_2, and C_3 are to be substituted into the ΔE_i^2 equation. After this computation, one must then relate the σ_{C_k} to σ_{E_0}, σ_Θ, and σ_Φ:

$$\sigma_{E_0}^2 = \sum_k [\left(\frac{\partial E_0}{\partial C_k}\right)^2 \sigma_{C_k}^2],$$

$$\sigma_\Theta^2 = \sum_k [\left(\frac{\partial \Theta}{\partial C_k}\right)^2 \sigma_{C_k}^2],$$

$$\text{and} \quad \sigma_\Phi^2 = \sum_k [\left(\frac{\partial \Phi}{\partial C_k}\right)^2 \sigma_{C_k}^2].$$

The resulting values of these σ_i can be seen in the error bars of Figures 29 and 30 (σ_{E_0}) and Table 3 (σ_Θ and σ_Φ). In Table 3, the *average* value of σ_Θ and σ_Φ over the continuous period indicated is shown. In this analysis, these σ_i have been

treated as independent, but in the case of σ_{E_0} and σ_Θ this is not quite so. It is not clear just how dependent σ_{E_0} is upon σ_Θ, because both the unknown background noise level and σ_{E_0} affect σ_Θ. Fortunately, this is not critical as the Earth fell outside a directional wedge in the Θ direction only once (on 27 December 1984), and that was only by $\sim 4°$.

The average σ_Φ for the complete set of measurements was about 1.59°, while the average value of σ_Θ overall was $\sim$ 3.28°. The values of σ_Φ for the separate periods of continuous emission varied from 2.17° to 1.22°. Similarly, the σ_Θ values were all between 3.80° and 2.09°. These errors are in reasonable agreement with the error values reported by other direction-finding analyses, notably Kurth *et al.* [1975]. This σ_Φ does not account for deviations from Earth of the source directions indicated on 27 December 1984 and 4-5 March 1986. On those days, the direction found had a tendency to point between the Earth and Sun. One possible explanation for this is that the Sun becomes a source comparable to the Earth in the 4.4 to 5.2 MHz frequency range, and therefore was also detected by the *IRM* [W. S. Kurth, personal communication]. This can easily change the value of Φ found by the fitting program to a point somewhere between the sources and becomes another systematic error that may have affected the direction-finding on those days.

These errors support the use of Equation 1 to adequately describe the observations and the determination of the Earth as the source of this emission.

CHAPTER V

ELECTRIC FIELD STRENGTH ANALYSIS

Up to this point, only the angular information calculated from Equation 1 has been considered. We now consider the electric field strengths calculated from the fitting program by using two methods of analysis: graphing the field strength against its radial distance from the Earth; and calculating the implied power of the source, assuming the radiation originates at the Earth. These methods may reveal more about the specific source of the radiation.

Electric Field Strength versus Radial Distance

If the source of the 4.8 MHz emission operates at a constant power, and the electric field intensity is not altered by the space between the source and the spacecraft, then the electric field strength of the emission should fall off with distance as $\frac{1}{r}$. With this relationship in mind, the common logarithm of the E_0 values obtained from each eight-minute segment of data were plotted against the common logarithm of the *IRM*'s radial distance from the Earth in Figure 29. A least squares fit to the measurements was applied to determine the slope of the calculated points and the correlation coefficient of the line calculated. (The correlation coefficient quantifies how well the line fits the data: values run from 0.0 (does not fit) to 1.0 (fits perfectly).) The figure here clearly rejects the hypothesis of a single, constant souce, radiating into empty space. Further examination of the separate sections of

continuous 4.8 MHz spin-correlated emission (Figure 30) show that there seems to be no correlation of any type whatsoever, implying that: 1) there is more than one source, 2) the source is highly variable in power, 3) the emission is being variably damped in the space between the source and the spacecraft, or 4) a combination of the above.

Power Analysis of the 4.8 MHz Radiation

To calculate the amount of power seen in the 4.8 MHz channel, the equation

$$P = \frac{2\pi R^2}{377} \int \left(\frac{E^2}{\Delta f} \right) df$$

was used, which gives the power in Watts if all the input values are also in MKS units. It is assumed here that the radiation originates from the Earth's surface. Thus, the distance of the *IRM* from the Earth is substituted for R and the surface area expression is $2\pi R^2$, because the source can only radiate into the hemisphere away from the Earth.

When this calculation was performed, the power of the spin-correlated emissions measured was found to vary from as little as 2.18 kW to as much as 4.33 MW. This is an extremely wide range. The maximum power is almost an order of magnitude larger than the power reported by LaBelle *et al.* [1989], who estimated the radiated power to be 500 kW. LaBelle *et al.* suggested that the radiation may be generated by over-the-horizon radars.

CHAPTER VI

CONCLUSIONS

From the previous analysis we arrive at the following conclusions:

1) the 4.8 MHz spin-correlated emission is a real emission,

2) the source of the 4.8 MHz spin-correlated emission is located on or near the Earth,

3) the source of the 4.8 MHz spin-correlated emission is *not* a single, constant source, unobscured by the space between its transmission and reception points, and

4) the 4.8 MHz spin-correlated emission can turn on or off suddenly, as would be expected from a human-made emission.

In the light of this evidence, the hypothesis that the radiation originates from the Earth is well-founded, though it is also obvious that the generating mechanism and/or propagating conditions are complex, be they human-made or not. LaBelle *et al.* suggested that over-the-horizon radar may be responsible for these events. Such a radar source is possible, provided that the transmitters went into operation sometime after 1980. At that time, the Defense Meteorological Satellite Program's *DMSP* satellite made a low orbit ($\sim$ 860 km) survey of radio power radiated from the Earth over the range of 1.2 to 13.9 MHz (see Rush *et al.* [1978, 1980]). Interpretation of the 1980 results indicates only about 18 kW of power in the same bandwidth at that time (unless these radars were turned off during *DMSP*'s passes).

Pirate radio stations are also a possibility, and there have also been some ionospheric heating experiments at experimental transmitters in Peru and Scandinavia, at the Aricebo radio telescope in Puerto Rico, and at the HIPAS installation in Alaska using frequencies quite near the frequencies we studied and power well in excess of 1 MW, so they, too, may have contributed to the emissions seen.

Although the locations of these sources on the Earth's surface cannot be pinpointed by the source wedges, they may be narrowed down by eliminating those parts of the Earth that the spacecraft could not see due to the Earth's rotation. Applying this idea revealed that *no* region of the Earth was visible every time the 4.8 MHz emission was detected by the *IRM*; thus, there must be more than one source. Sightings of the emission occurred when the spacecraft was over South America, the Pacific and Indian Oceans, and Indonesia.

Regardless of the specific source or sources, however, it seems certain that the source itself is located on or very near to the Earth.

REFERENCES

Bernhardt, P. A., Roussel-Dupre, R. A., Pongratz, M. B., Haerendel, G., Valenzuela, A., Gurnett, D. A., and Anderson, R. R., 1987, *J. Geophys. Res.*, **92**, 5777-94.

Bevington, P. R., 1969, *Data Reduction and Error Analysis for the Physical Sciences* (McGraw-Hill), p. 222-5.

Gurnett, D. A., Anderson, R. R., Bernhardt, P. A., Lühr, H., Haerendel, G., Bauer, O. H., Treumann, R. A., Koons, H. C., and Holzworth, R. H., 1986, *Geophys. Res. Lett.*, **13**, 644-7.

Gurnett, D. A., Anderson, R. R., Häusler, B., Haerendel, G., Bauer, O. H., Koons, H. C., Treumann, R. A., Holzworth, R. H., and Lühr, H., 1985, *Geophys. Res. Lett.*, **12**, 851-4.

Gurnett, D. A., Anderson, R. R., Ma, T. Z., Haerendel, G., Paschmann, G., Bauer, O. H., Treumann, R. A., Koons, H. C., Holzworth, R. H., and Lühr, H., 1986, *J. Geophys. Res.*, **91**, 10013-28.

Häusler, B., Anderson, R. R., Gurnett, D. A., Koons, H. C., Holtzworth, R. H., Bauer, O. H., Treumann, R., Gnaiger, K., Odem, D., Harbridge, W. B., and Eberl, F., 1985, in *I. E. E. E. Trans. Geosci. Remote Sens.*, *GE-23*, 267.

Kurth, W. S., Baumback, M. M., and Gurnett, D. A., 1975, *Geophys. Res. Lett.*, **80**, 2764-70.

LaBelle, J., Treumann, R. A., Boehm, M. H., Gewecke, K., 1989, *Radio Science*, **24**, 725-37.

Rush, C. M., Nelson, D., Snyder, A. L., Patterson, V., Tascione, T., and Ziemba, E., 1978, in *Effect of the Ionosphere on Space and Terrestrial systems*, ed. J. M. Goodman, p. 183-7.

Rush, C. M., Snyder, A. L., Ziemba, E., Patterson, V., Tascione, T., and Nelson, D., 1980, *Radio Science*, **15**, 1127-36.

Russell, C. T., 1971, *Cosmic Electrodynamics*, **2**, 184-96.

APPENDIX I: TABLES

Table 1. Periods for which high-frequency electric field data from the *AMPTE IRM* spacecraft were available for this study.

Observation Date	Observation Interval
27 December 1984	84:362:1100:15–1454:01
21 April 1985	85:111:0024:05–0236:34
25 April 1985	85:116:0554:52–0736:51
8 June 1985	85:159:1132:00–2214:02
9 June 1985	85:160:1711:58–1727:40
4-5 March 1986	86:063:2209:39–064:0441:58*

* (101 kHz–706 kHz data ended at 063:2309:48)

Table 2. Periods for which the data in the 4.8 MHz band of the high-frequency electric field receiver of the *AMPTE IRM* spacecraft showed a spin-correlated signal.

Observation Date	4.8 MHz Signal Interval(s)
27 December 1984	84:362:1100:15–1215:20
21 April 1985	85:111:0024:05–0236:34
26 April 1985	none
8 June 1985	85:159:1245:00–1500:00 85:159:1546:02–2204:37
9 June 1985	85:160:1711:58–1727:40
4-5 March 1986	86:063:2216:49–064:0014:01 86:064:0309:24–0441:58

Table 3. Average σ_Θ and σ_Φ values for each period that displayed a spin-correlated signal in the *AMPTE IRM* 4.8 MHz high-frequency electric field receiver band.

4.8 MHz Signal Interval	σ_Θ (°)	σ_Φ (°)
84:362:1100:15–1215:20	3.66	2.17
85:111:0024:05–0236:34	3.20	1.47
85:159:1245:00–1500:00	3.28	1.59
85:159:1546:02–2204:37	3.00	1.64
85:160:1711:58–1727:40	2.09	1.22
86:063:2216:49–064:0014:01	3.80	1.79
86:064:0309:24–0441:58	3.48	1.36
Average of all measurements	3.28	1.59

APPENDIX II: FIGURES

Figure 1. Line drawing of the *AMPTE IRM* spacecraft.

C-G81-560

AMPTE ION RELEASE MODULE

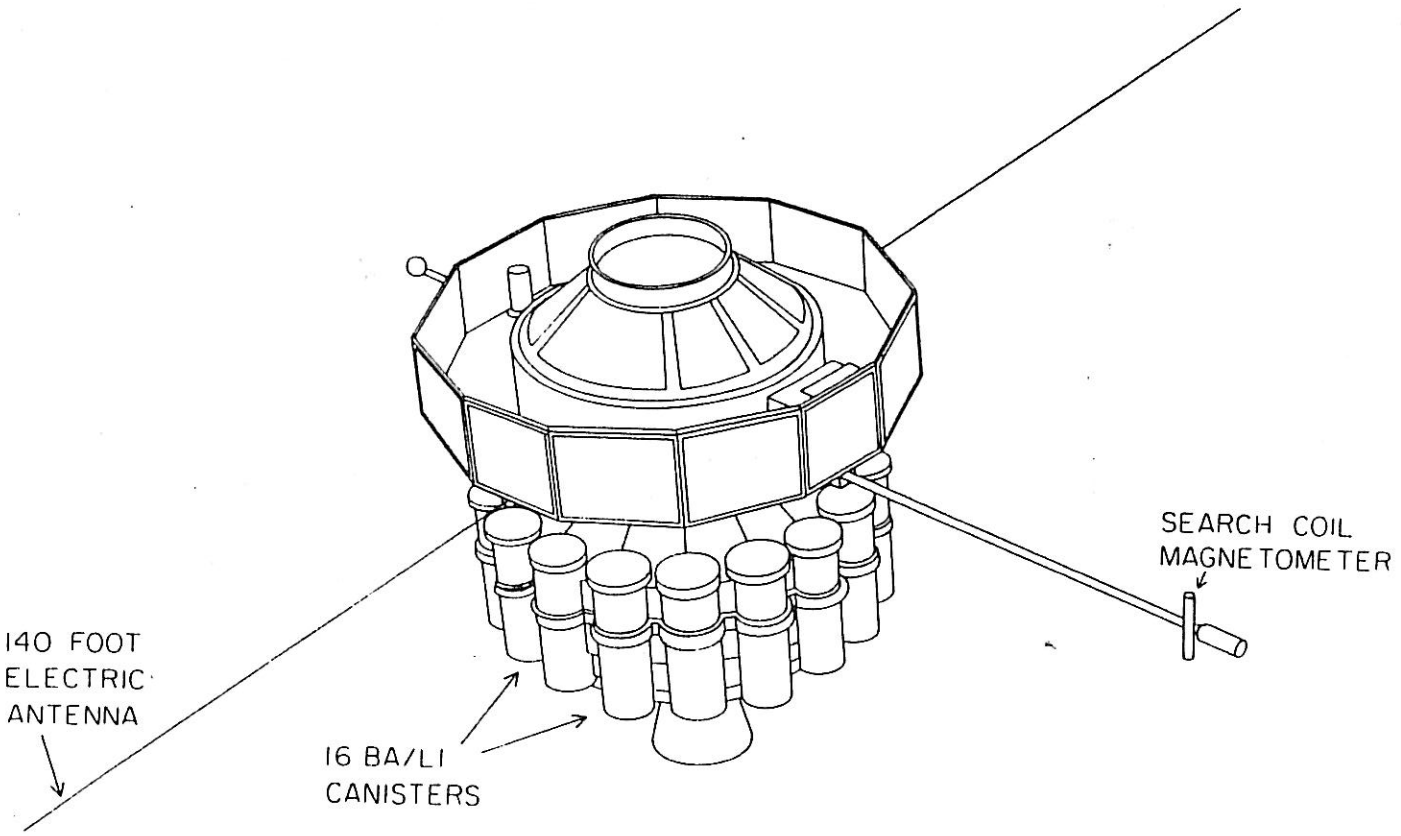

Figure 2. Spectrogram of the *AMPTE IRM* barium release on 27 December 1984. The range of the intensity scale runs from the instrument noise level (dark blue) to the receiver's saturation level (red). Note the plasma frequency cutoff by the cloud's electrons, and its effect on the band of interest, the intense, narrow band at the top of the spectrogram.

A-G86-331

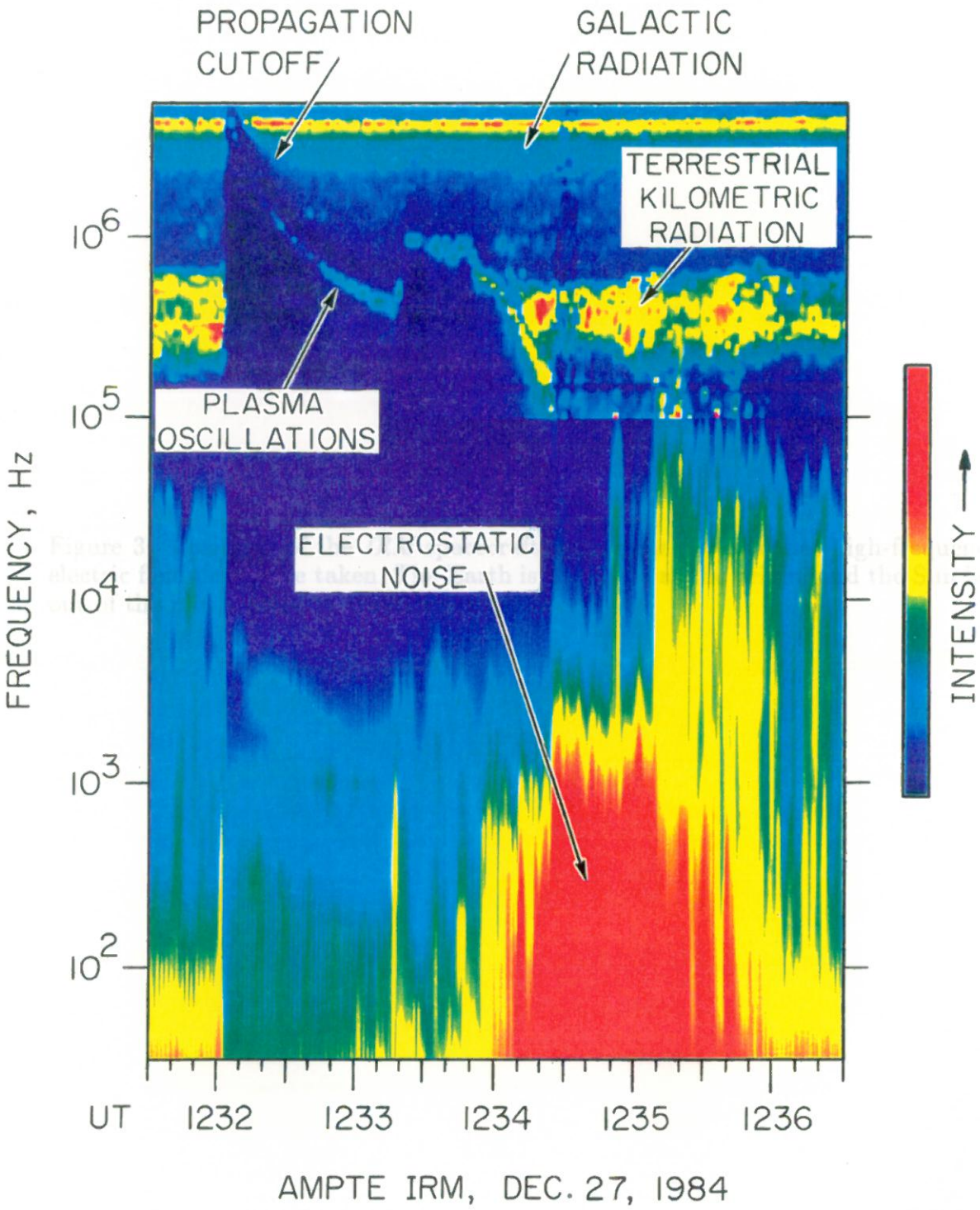
PROPAGATION CUTOFF
GALACTIC RADIATION
TERRESTRIAL KILOMETRIC RADIATION
PLASMA OSCILLATIONS
ELECTROSTATIC NOISE
FREQUENCY, Hz
10^6
10^5
10^4
10^3
10^2
INTENSITY
UT
1232
1233
1234
1235
1236
AMPTE IRM, DEC. 27, 1984

Figure 3. Positions of the *IRM* spacecraft during the periods that high-frequency electric field data were taken. The Earth is the circle at the origin, and the Sun lies out of the plot, down the positive x-axis.

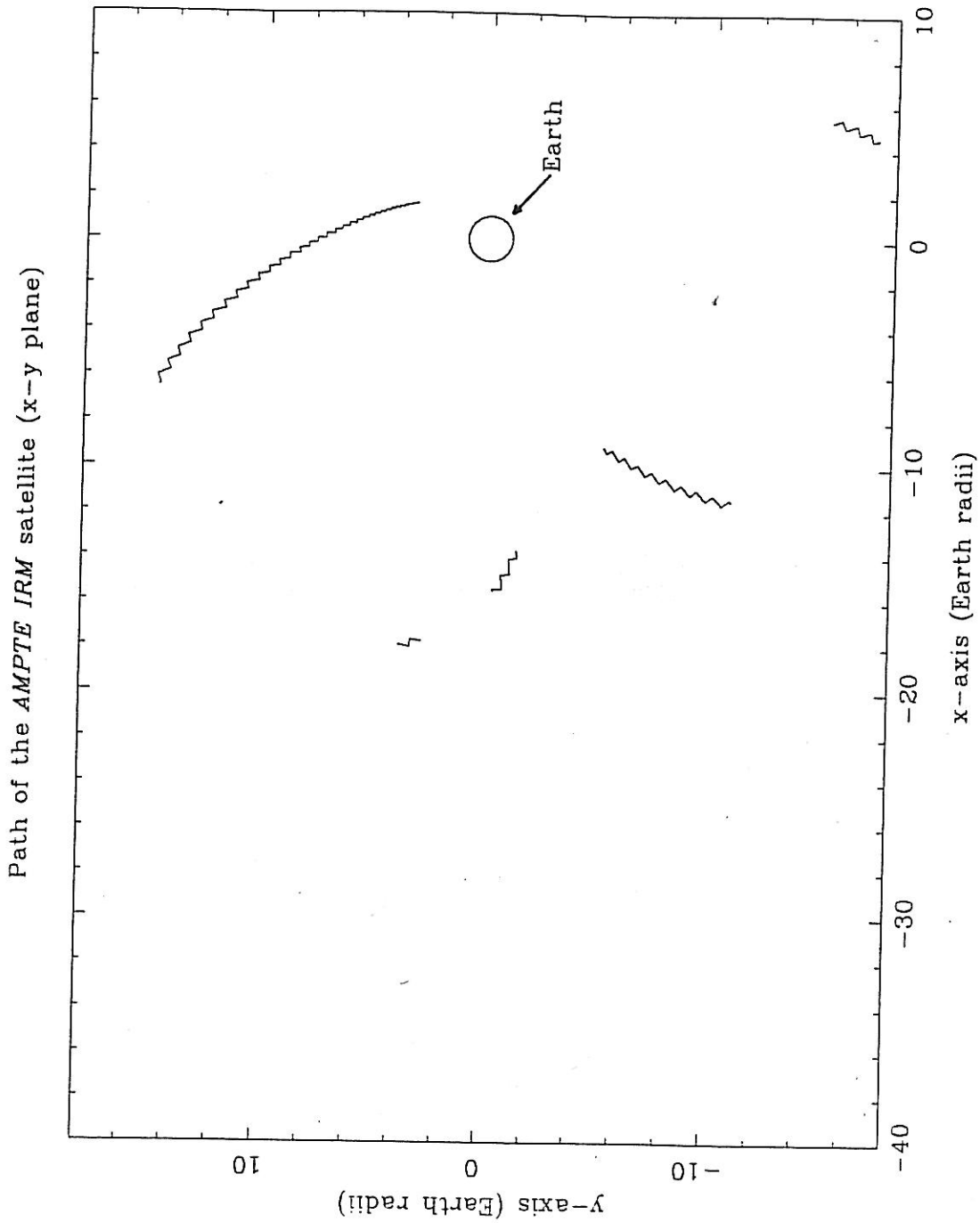
Path of the AMPTE IRM satellite (x-y plane)
Earth
y-axis (Earth radii)
x-axis (Earth radii)
10
0
-10
10
0
-10
-20
-30
-40

Figure 4. Common logarithm of the electric field strength versus time on 8 June 1985 to demonstrate an instance where the signal suddenly disappears.

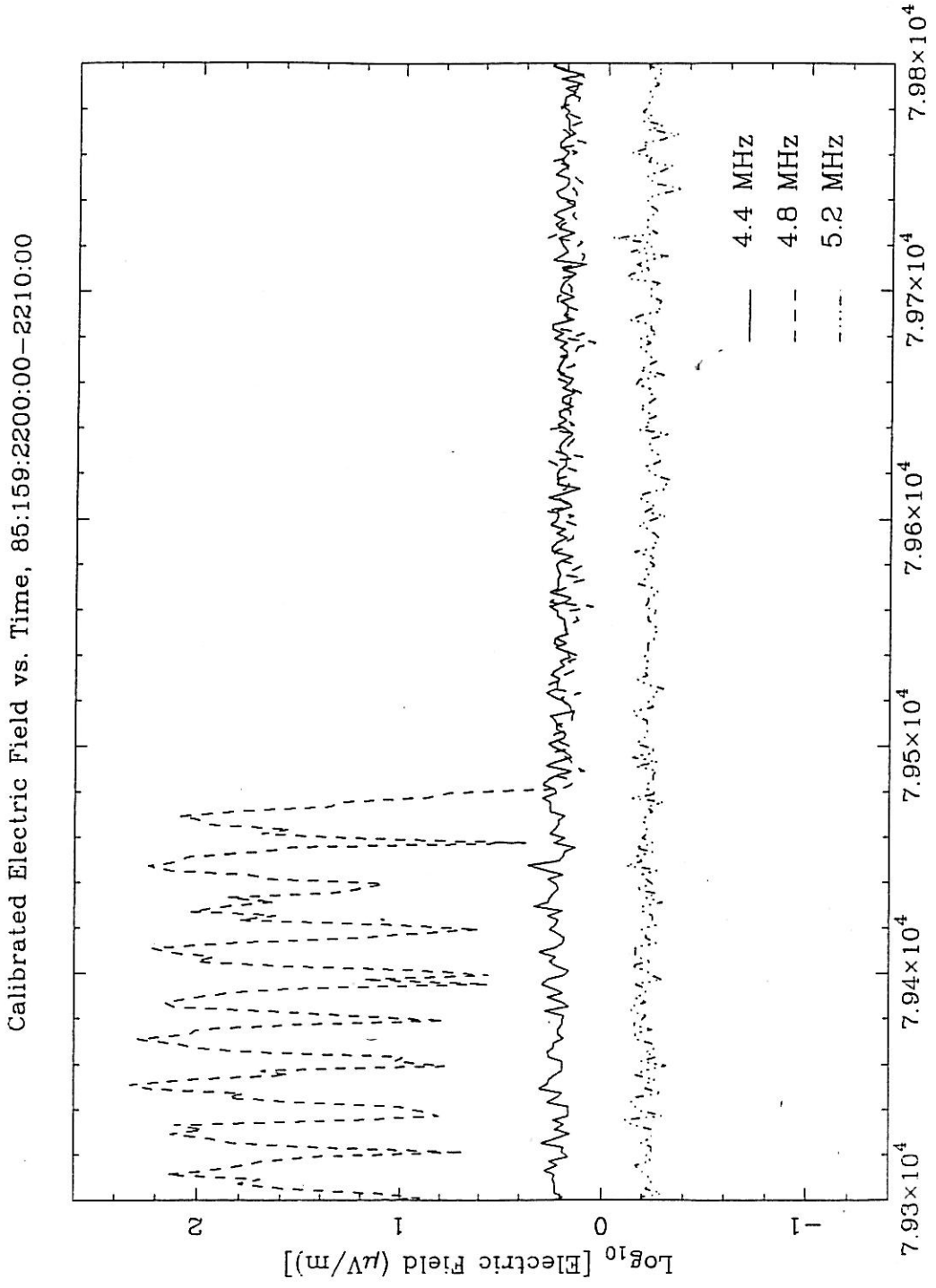
Calibrated Electric Field vs. Time, 85:159:2200:00–2210:00
Log10 [Electric Field (μV/m)]
2
1
0
−1
7.93×10^4
7.94×10^4
7.95×10^4
7.96×10^4
7.97×10^4
7.98×10^4
Time of Day (sec)
4.4 MHz
4.8 MHz
5.2 MHz

Figure 5. Common logarithm of the electric field strength versus time on 5 March 1986 to demonstrate an instance where the signal abruptly appears.

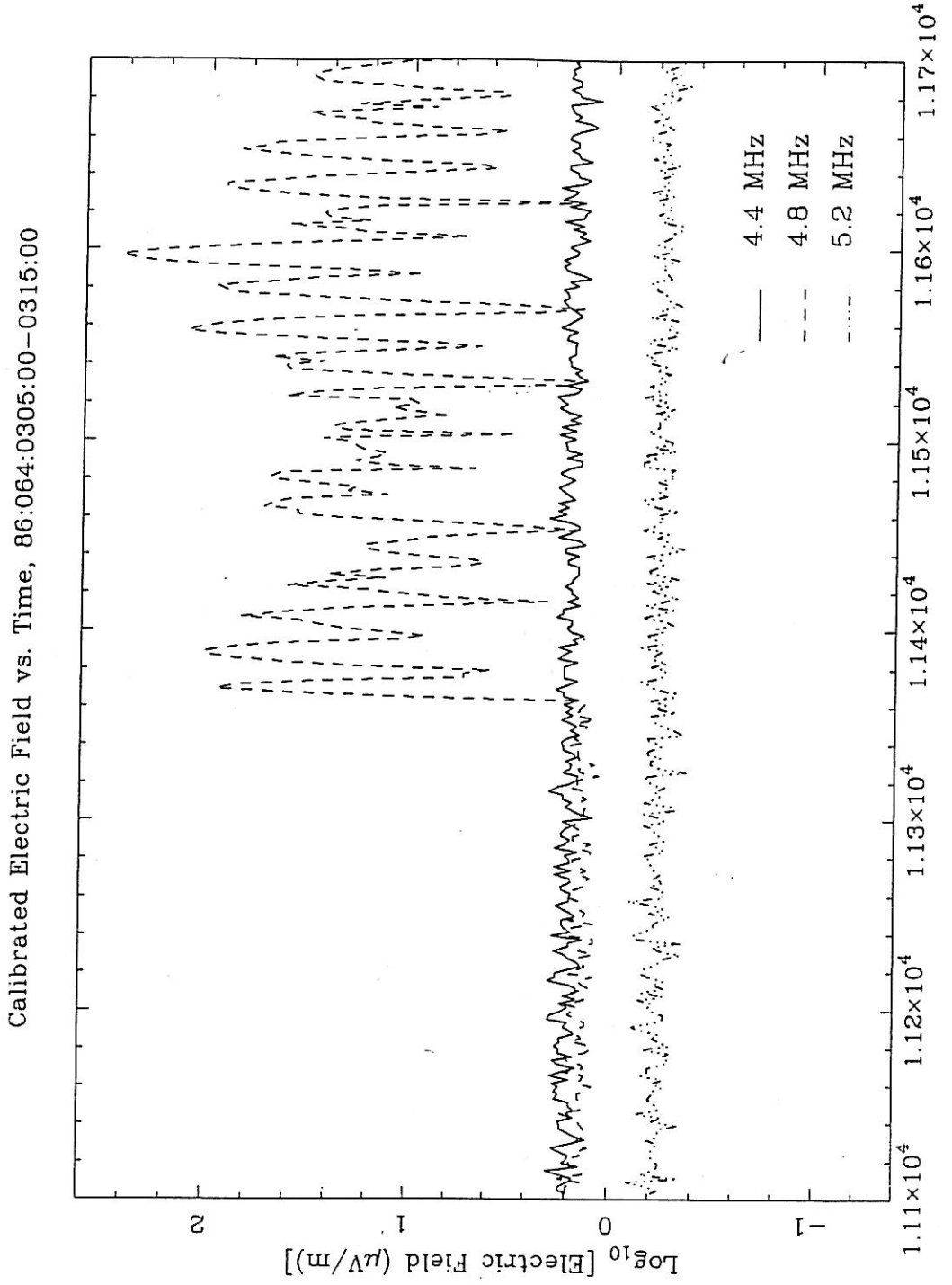
Calibrated Electric Field vs. Time, 86:064:0305:00–0315:00
Log10 [Electric Field (μV/m)]
2
1
0
−1
1.11×10^4
1.12×10^4
1.13×10^4
1.14×10^4
1.15×10^4
1.16×10^4
1.17×10^4
Time of Day (sec)
4.4 MHz
4.8 MHz
5.2 MHz

Figure 6. Polar (left) and rectangular plots of a simulated strong ($\sim$ 100 μV/m) source at $\Theta = 89.95°$, $\Phi = 65°$ (the solid line) with an omnidirectional background noise level of $\sim$ 2.4 μV/m (the dashed line). The open circles represent sample data points under this combined field. Note how the background noise fills the notches where the antenna alignment results in minimum reception.

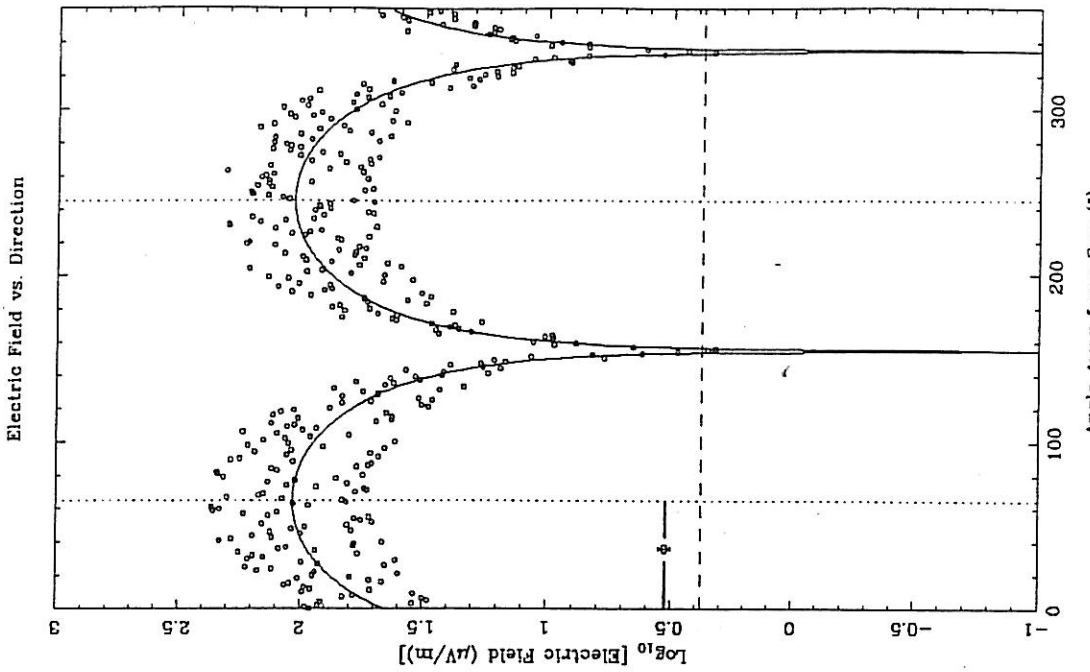
Electric Field vs. Direction
Angle Away from Sun (°)
Log10 [Electric Field (μV/m)]
0
100
200
300
−1
−0.5
0
0.5
1
1.5
2
2.5
3
Φ

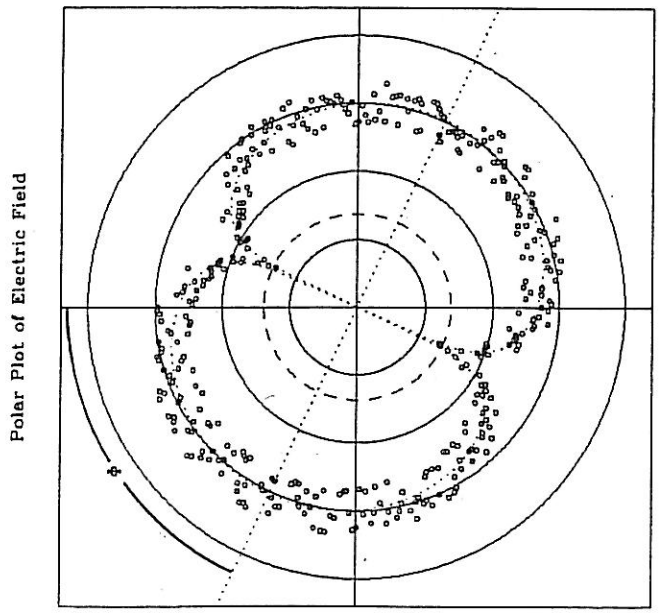
Polar Plot of Electric Field
Φ

Figure 7. Polar (left) and rectangular plots of a simulated weak ($\sim$ 8.4 μV/m) source at $\Theta = 89.3°$, $\Phi = 65°$ (the solid line) with an omnidirectional background noise level of $\sim$ 2.4 μV/m (the dashed line). The open circles represent sample data points under this combined field. Note how the background noise fills the notches where the antenna alignment results in minimum reception.

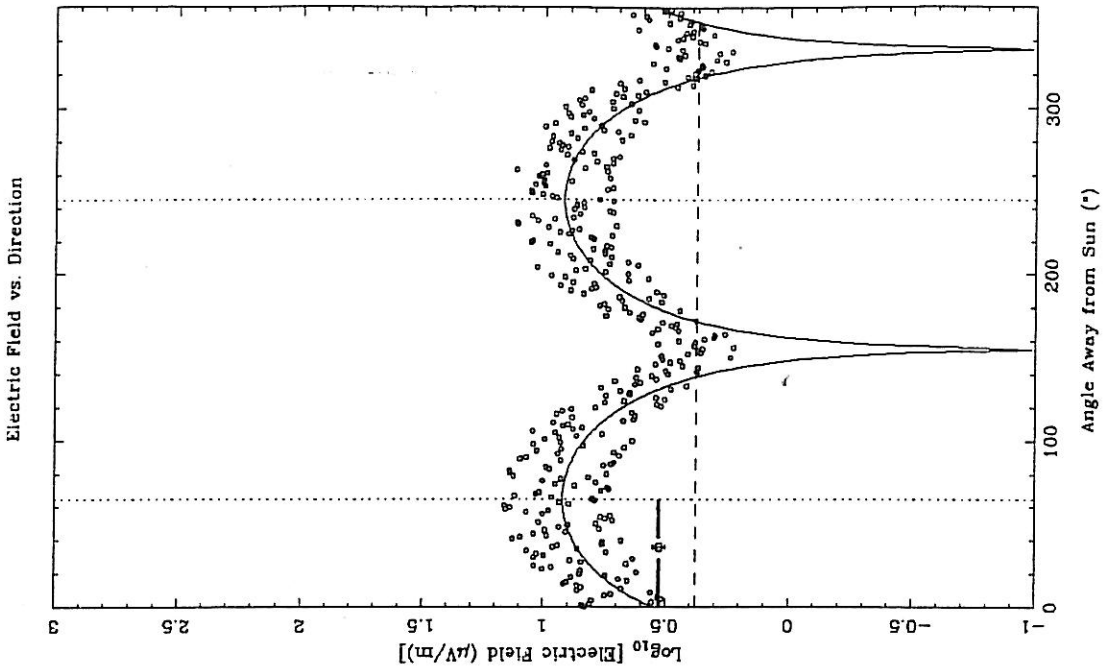
Electric Field vs. Direction
Angle Away from Sun (°)
$\log_{10}$ [Electric Field (μV/m)]
0
100
200
300
−1
−0.5
0
0.5
1
1.5
2
2.5
3

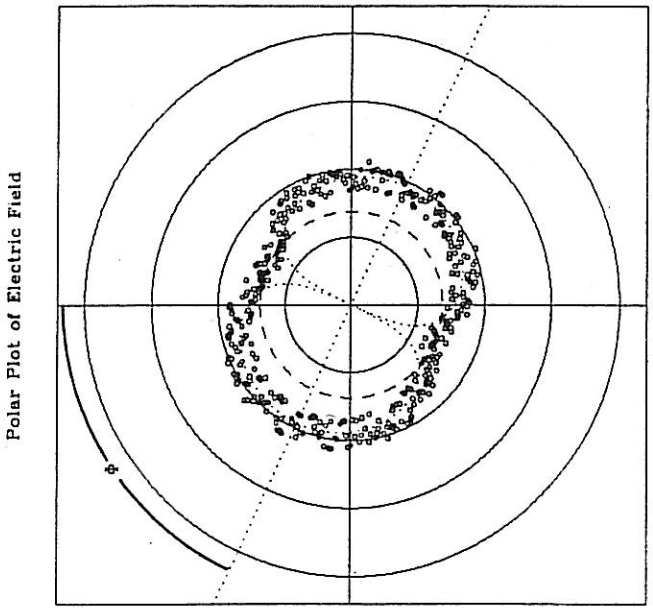
Polar Plot of Electric Field

Figure 8. Polar (top) and rectangular plots of the 4.4, 4.8, and 5.2 (left to right) MHz bands for an arbitrary eight-minute period on 27 December 1984 where a spin-correlated signal was seen in the 4.8 MHz channel.

Polar Plot of 4.4 MHz Electric Field for Day 362, 1984

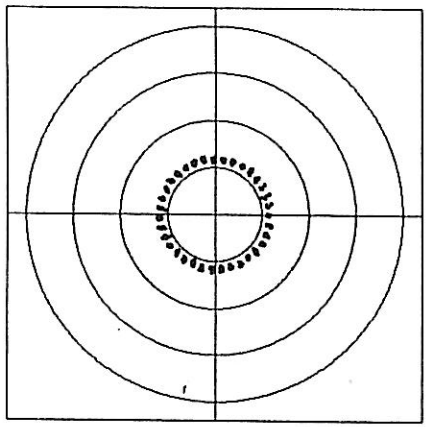

1150:01--1157:59

Polar Plot of 4.8 MHz Electric Field for Day 362, 1984

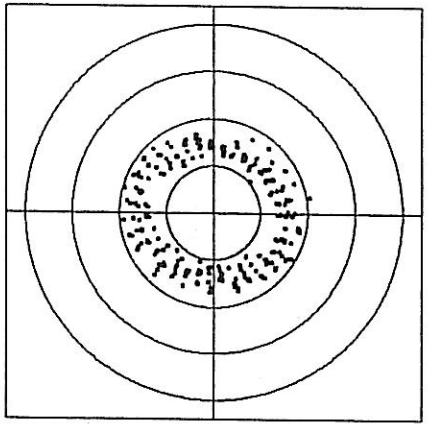

1150:01--1157:59

Polar Plot of 5.2 MHz Electric Field for Day 362, 1984

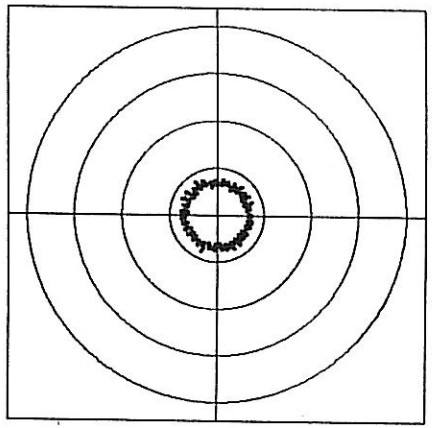

1150:01--1157:59

4.4 MHz Electric Field vs. Direction for Day 362, 1984

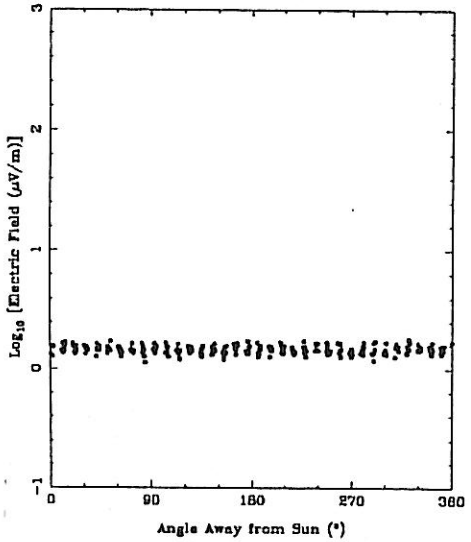

4.8 MHz Electric Field vs. Direction for Day 362, 1984

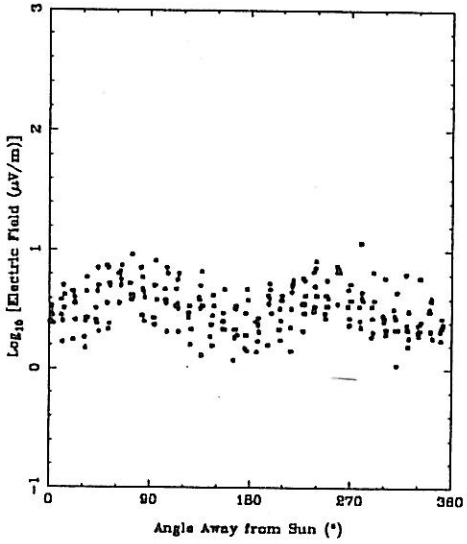

5.2 MHz Electric Field vs. Direction for Day 362, 1984

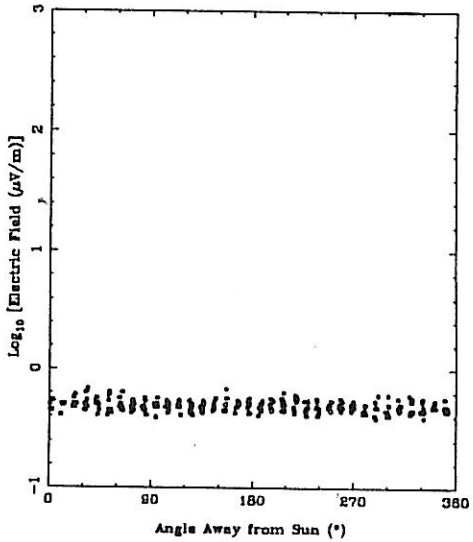

Figure 9. Polar (top) and rectangular plots of the 4.4, 4.8, and 5.2 (left to right) MHz bands for an arbitrary eight-minute period on 21 April 1985 where a spin-correlated signal was seen in the 4.8 MHz channel.

Polar Plot of 4.4 MHz Electric Field for Day 111, 1985

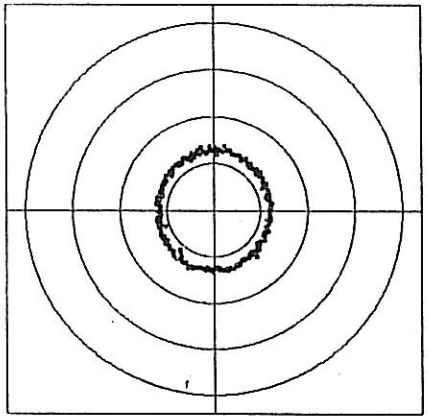

0110:01--0117:59

Polar Plot of 4.8 MHz Electric Field for Day 111, 1985

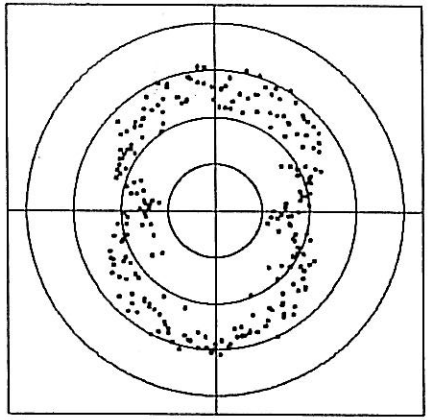

0110:01--0117:59

Polar Plot of 5.2 MHz Electric Field for Day 111, 1985

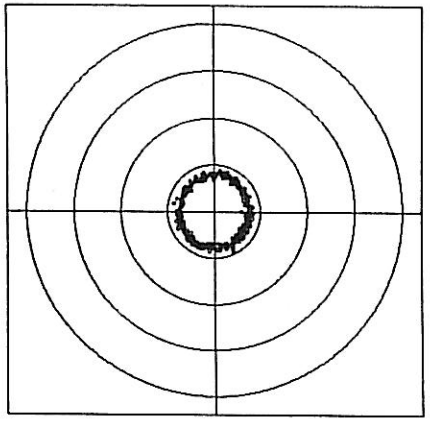

0110:01--0117:59

4.4 MHz Electric Field vs. Direction for Day 111, 1985

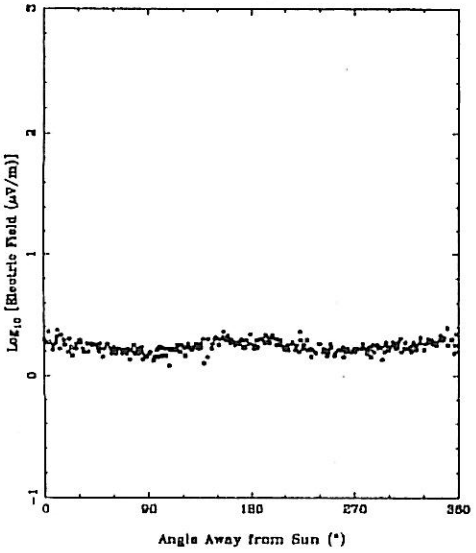

4.8 MHz Electric Field vs. Direction for Day 111, 1985

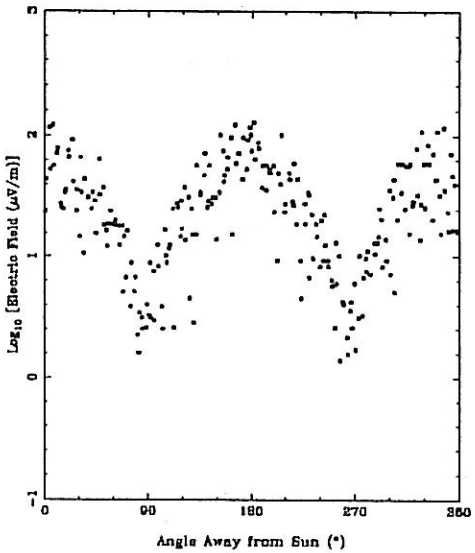

5.2 MHz Electric Field vs. Direction for Day 111, 1985

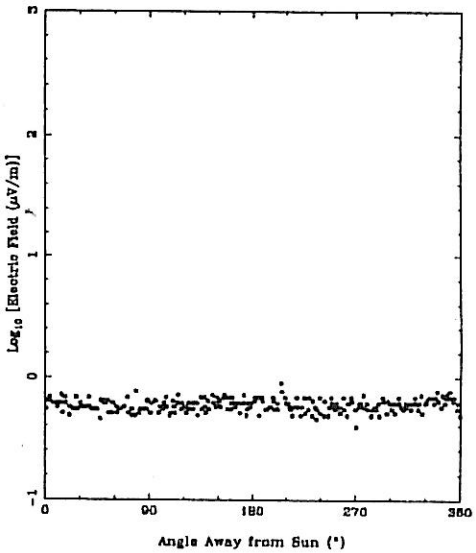

Figure 10. Polar (top) and rectangular plots of the 4.4, 4.8, and 5.2 (left to right) MHz bands for an arbitrary eight-minute period on 26 April 1985. On this day, no spin-correlated signal was seen in the 4.8 MHz band.

Polar Plot of 4.4 MHz Electric Field for Day 116, 1985

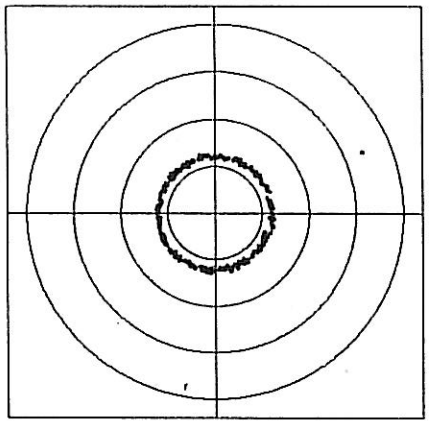

0820:01--0827:59

Polar Plot of 4.6 MHz Electric Field for Day 116, 1985

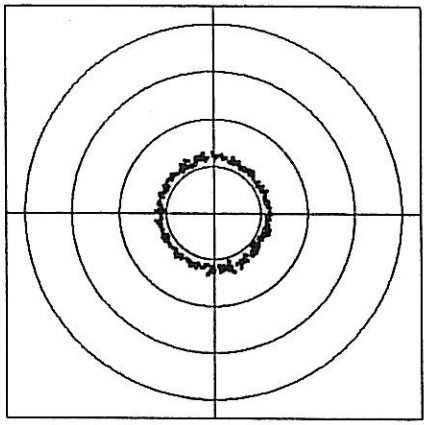

0820:01--0827:59

Polar Plot of 5.2 MHz Electric Field for Day 116, 1985

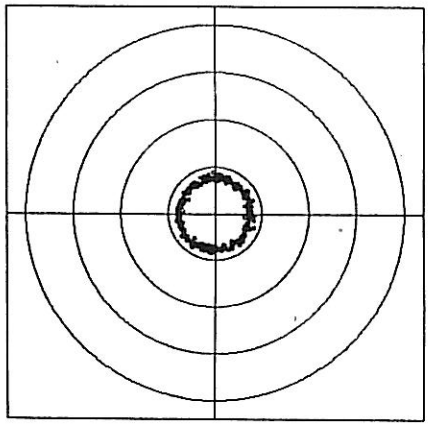

0820:01--0827:59

4.4 MHz Electric Field vs. Direction for Day 116, 1985

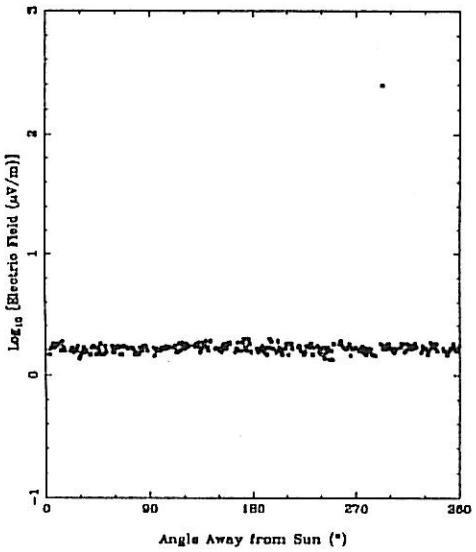

4.6 MHz Electric Field vs. Direction for Day 116, 1985

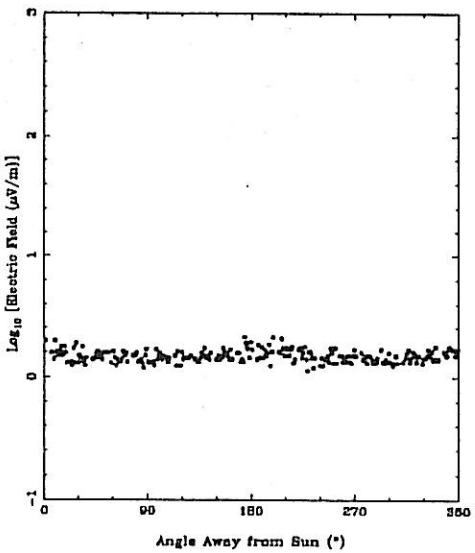

5.2 MHz Electric Field vs. Direction for Day 116, 1985

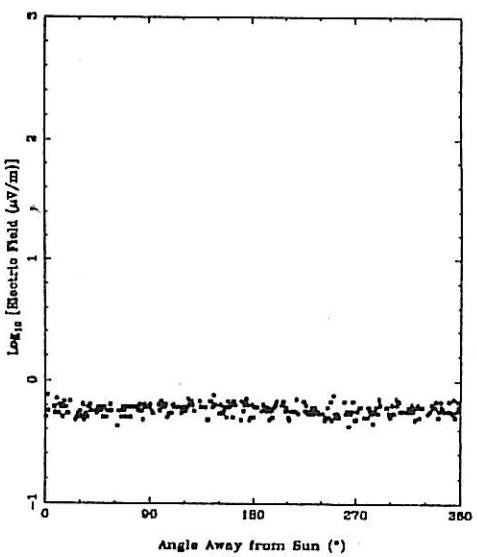

Figure 11. Polar (top) and rectangular plots of the 4.4, 4.8, and 5.2 (left to right) MHz bands for an arbitrary eight-minute period on 8 June 1985 where a spin-correlated signal was seen in the 4.8 MHz channel.

Polar Plot of 4.4 MHz Electric Field for Day 159, 1985

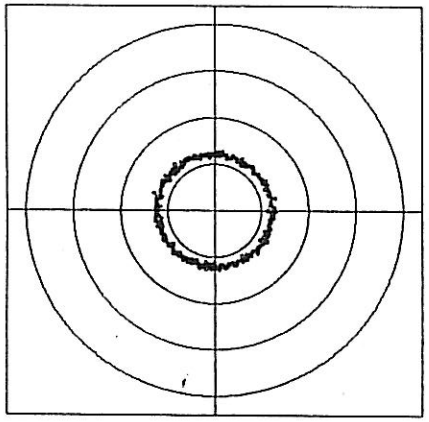

1840:00--1847:58

Polar Plot of 4.8 MHz Electric Field for Day 159, 1985

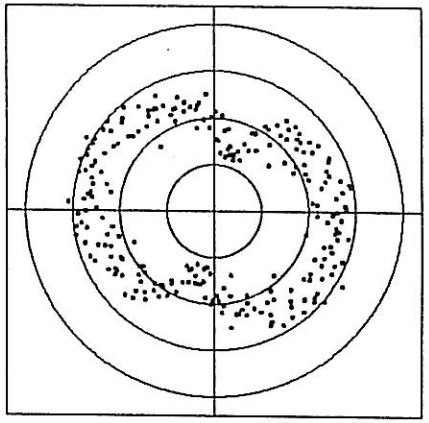

1840:00--1847:58

Polar Plot of 5.2 MHz Electric Field for Day 159, 1985

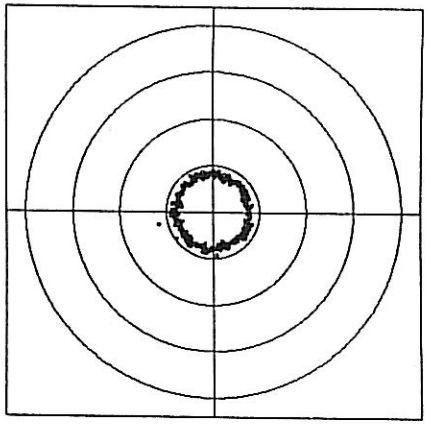

1840:00--1847:58

4.4 MHz Electric Field vs. Direction for Day 159, 1985

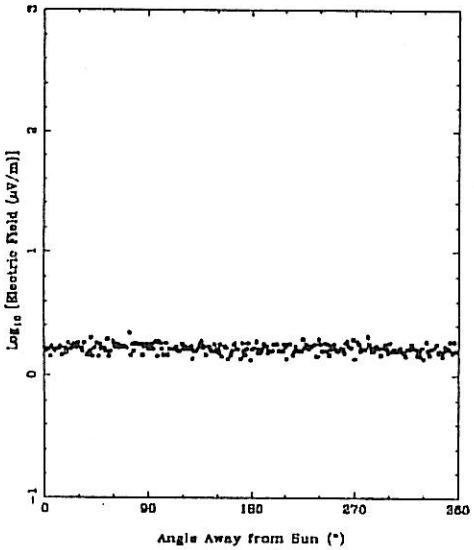

4.8 MHz Electric Field vs. Direction for Day 159, 1985

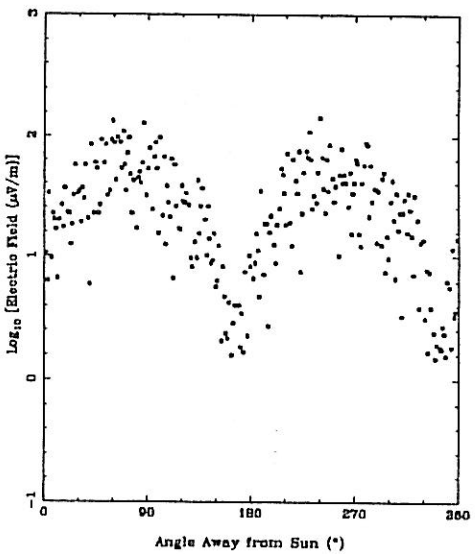

5.2 MHz Electric Field vs. Direction for Day 159, 1985

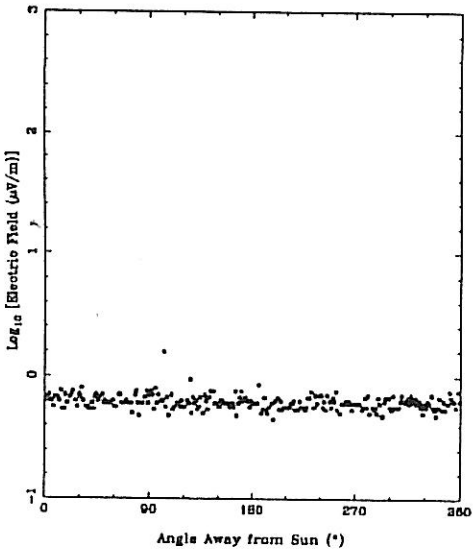

Figure 12. Polar (top) and rectangular plots of the 4.4, 4.8, and 5.2 (left to right) MHz bands for an arbitrary eight-minute period on 9 June 1985 where a spin-correlated signal was seen in the 4.8 MHz channel.

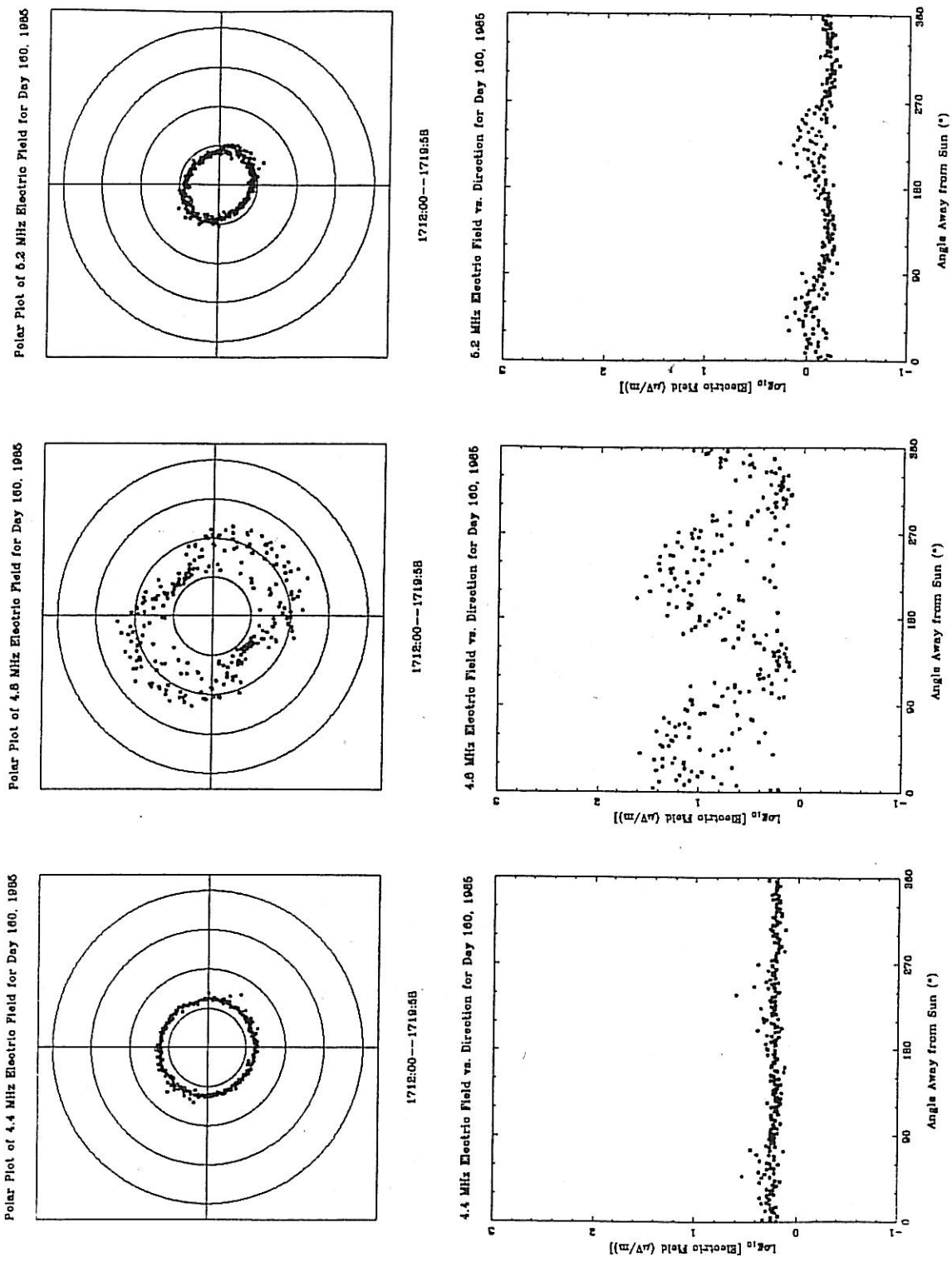
Polar Plot of 4.4 MHz Electric Field for Day 160, 1985
1712:00---1719:58
Polar Plot of 4.8 MHz Electric Field for Day 160, 1985
1712:00---1719:58
Polar Plot of 5.2 MHz Electric Field for Day 160, 1985
1712:00---1719:58
4.4 MHz Electric Field vs. Direction for Day 160, 1985
4.8 MHz Electric Field vs. Direction for Day 160, 1985
5.2 MHz Electric Field vs. Direction for Day 160, 1985
log10 [Electric Field (μV/m)]
Angle Away from Sun (°)
0
90
180
270
360
-1
0
1
2
3

Figure 13. Polar (top) and rectangular plots of the 4.4, 4.8, and 5.2 (left to right) MHz bands for an arbitrary eight-minute period on 5 March 1986 where a spin-correlated signal was seen in the 4.8 MHz channel.

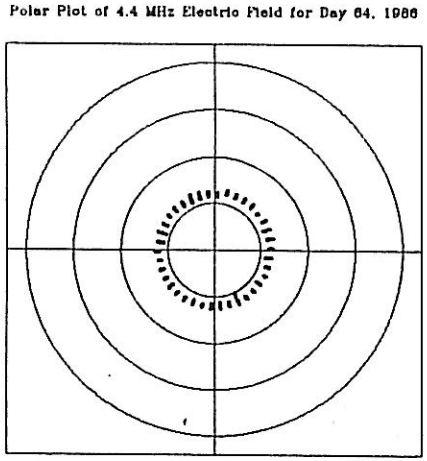
Polar Plot of 4.4 MHz Electric Field for Day 64, 1986
0312:00--0319:58

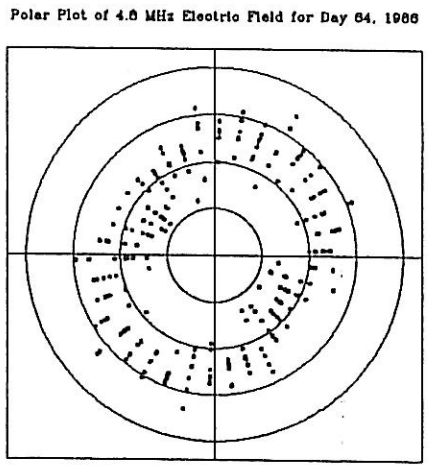
Polar Plot of 4.6 MHz Electric Field for Day 64, 1986
0312:00--0319:58

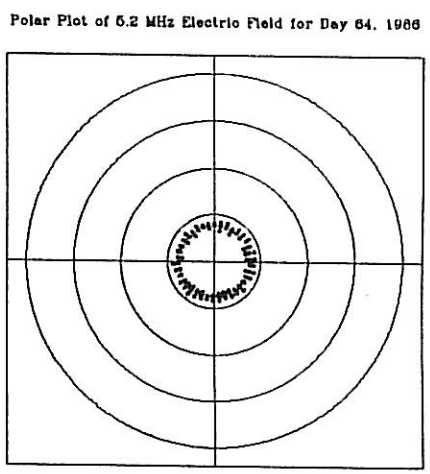
Polar Plot of 5.2 MHz Electric Field for Day 64, 1986
0312:00--0319:58

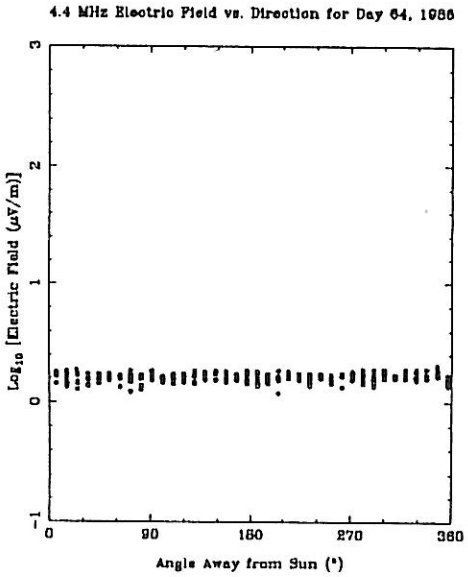
4.4 MHz Electric Field vs. Direction for Day 64, 1986
Log10 [Electric Field (μV/m)]
Angle Away from Sun (°)

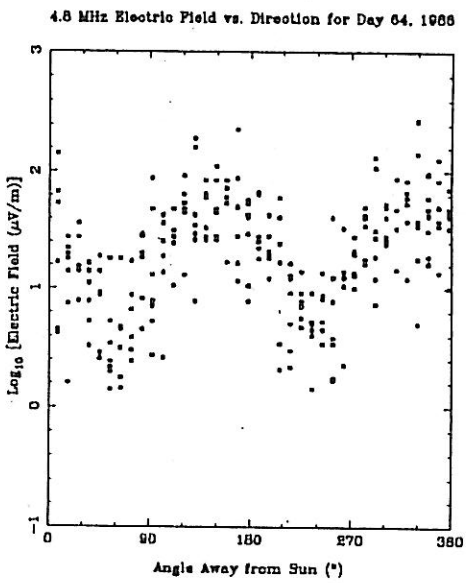
4.6 MHz Electric Field vs. Direction for Day 64, 1986
Log10 [Electric Field (μV/m)]
Angle Away from Sun (°)

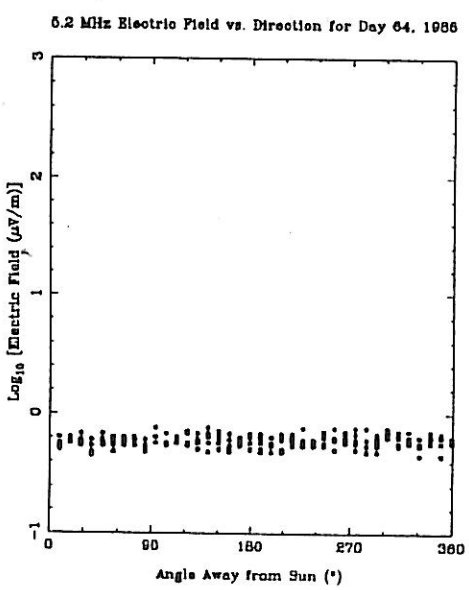
5.2 MHz Electric Field vs. Direction for Day 64, 1986
Log10 [Electric Field (μV/m)]
Angle Away from Sun (°)

Figure 14. Direction of the source of the spin-correlated 4.8 MHz data in the *IRM*'s spin plane on 27 December 1984. The projection of the Earth in this plane is denoted by the circle drawn, the projection of the spacecraft's course is the jagged line indicated, and the source directions are the dotted lines running between them.

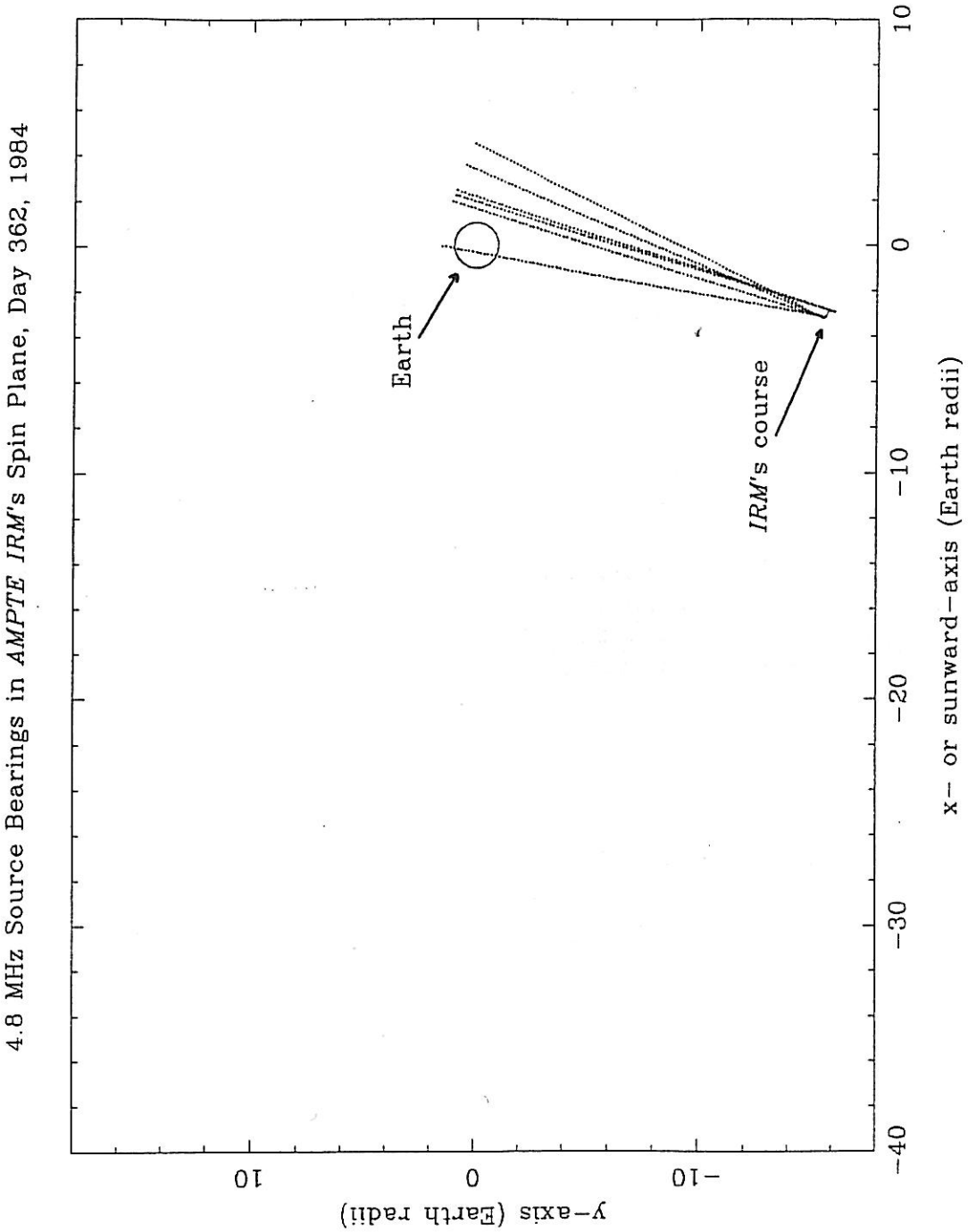
4.8 MHz Source Bearings in AMPTE IRM's Spin Plane, Day 362, 1984
Earth
IRM's course
y-axis (Earth radii)
x- or sunward-axis (Earth radii)
10
0
-10
10
0
-10
-20
-30
-40

Figure 15. Direction of the source of the spin-correlated 4.8 MHz data in the *IRM*'s spin plane on 21 April 1985. The projection of the Earth in this plane is denoted by the circle drawn, the projection of the spacecraft's course is the jagged line indicated, the source directions are the dotted lines running between them.

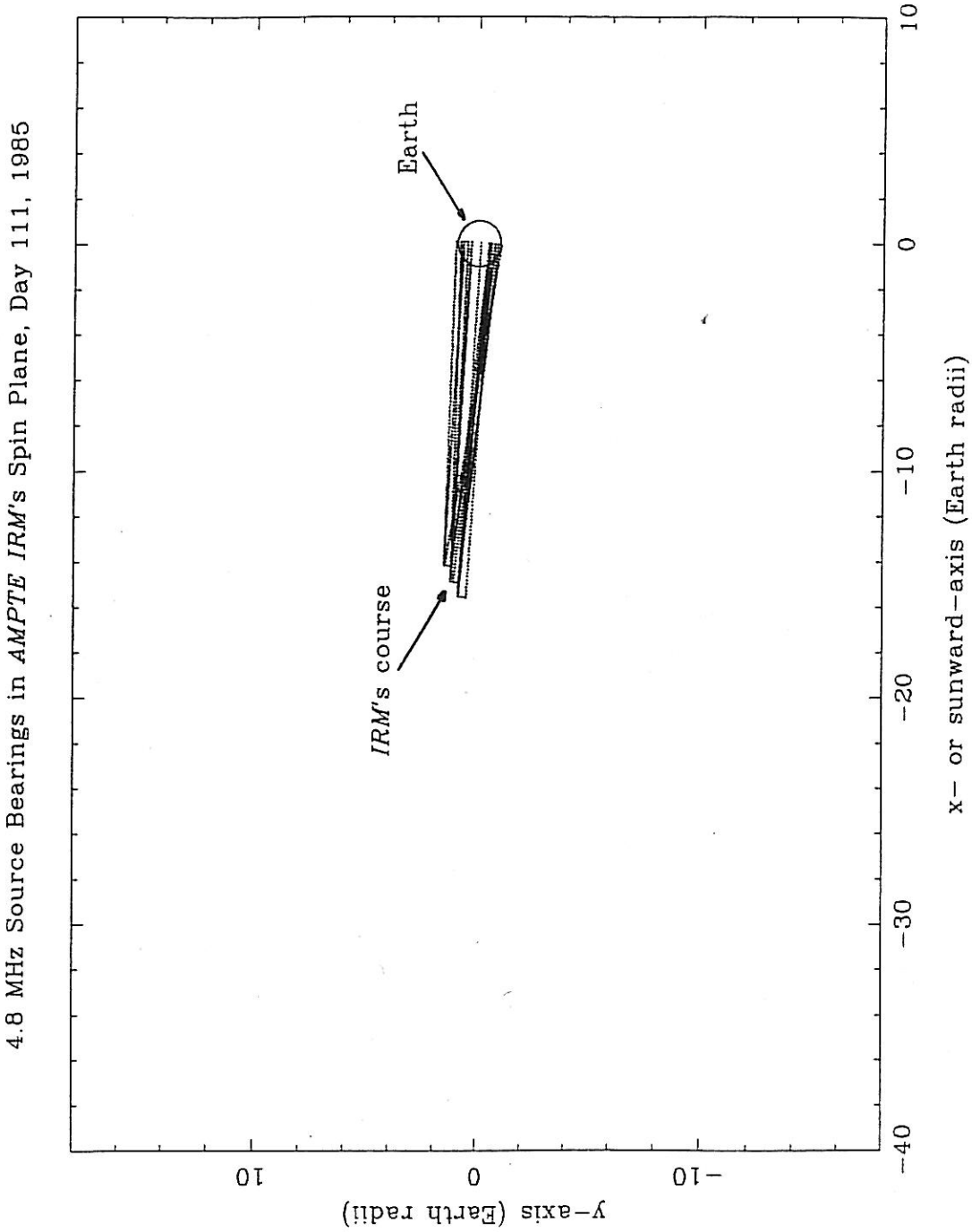
4.8 MHz Source Bearings in AMPTE IRM's Spin Plane, Day 111, 1985
Earth
IRM's course
y-axis (Earth radii)
10
0
-10
x- or sunward-axis (Earth radii)
10
0
-10
-20
-30
-40

Figure 16. Direction of the source of the spin-correlated 4.8 MHz data in the *IRM*'s spin plane on 8 June 1985. The projection of the Earth in this plane is denoted by the circle drawn, the projection of the spacecraft's course is the jagged line indicated, and the source directions are the dotted lines running between them.

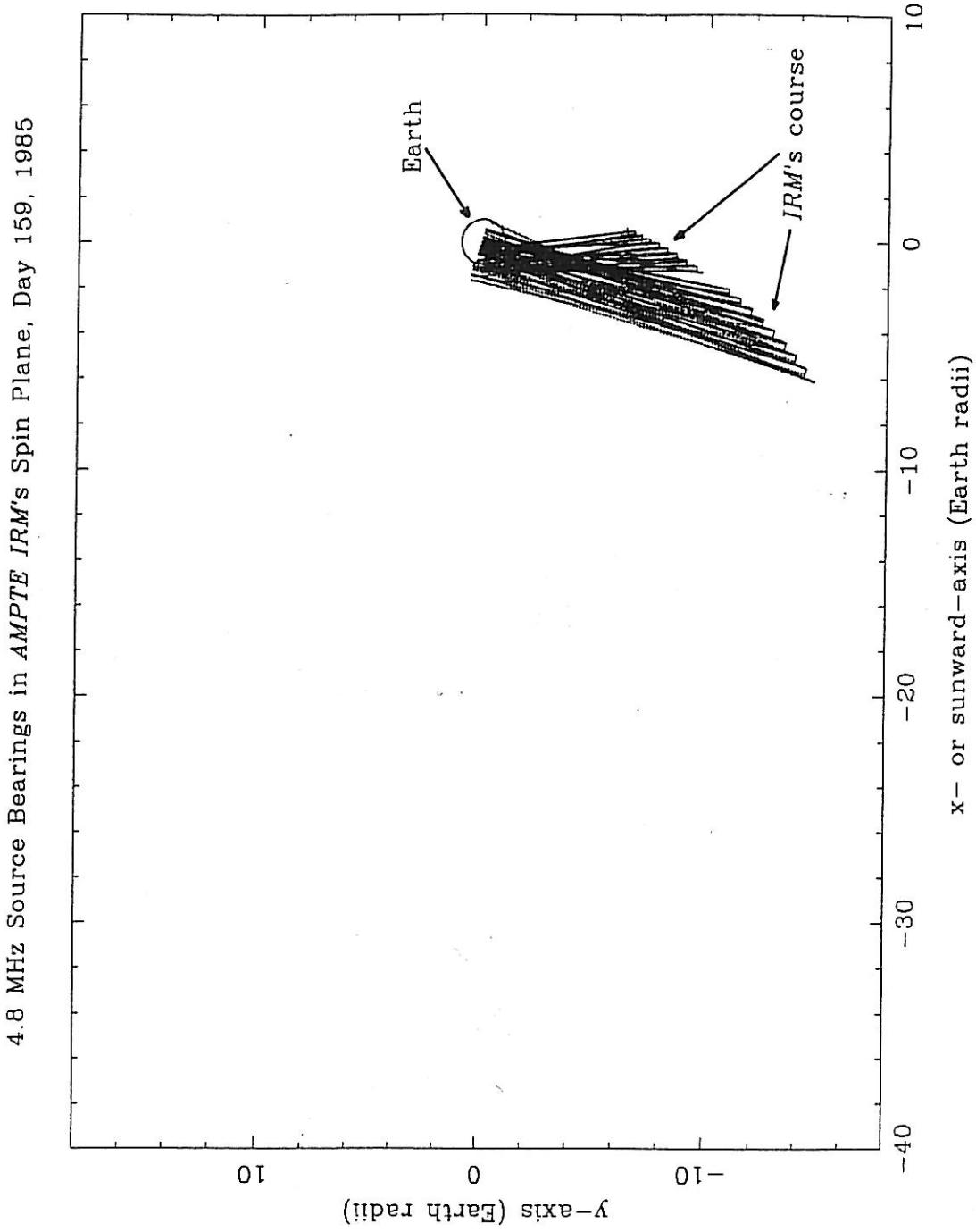
4.8 MHz Source Bearings in AMPTE IRM's Spin Plane, Day 159, 1985
Earth
IRM's course
y-axis (Earth radii)
x- or sunward-axis (Earth radii)
10
0
-10
10
0
-10
-20
-30
-40

Figure 17. Direction of the source of the spin-correlated 4.8 MHz data in the *IRM*'s spin plane on 9 June 1985. The projection of the Earth in this plane is denoted by the circle drawn, the projection of the spacecraft's course is the jagged line indicated, and the source directions are the dotted lines running between them.

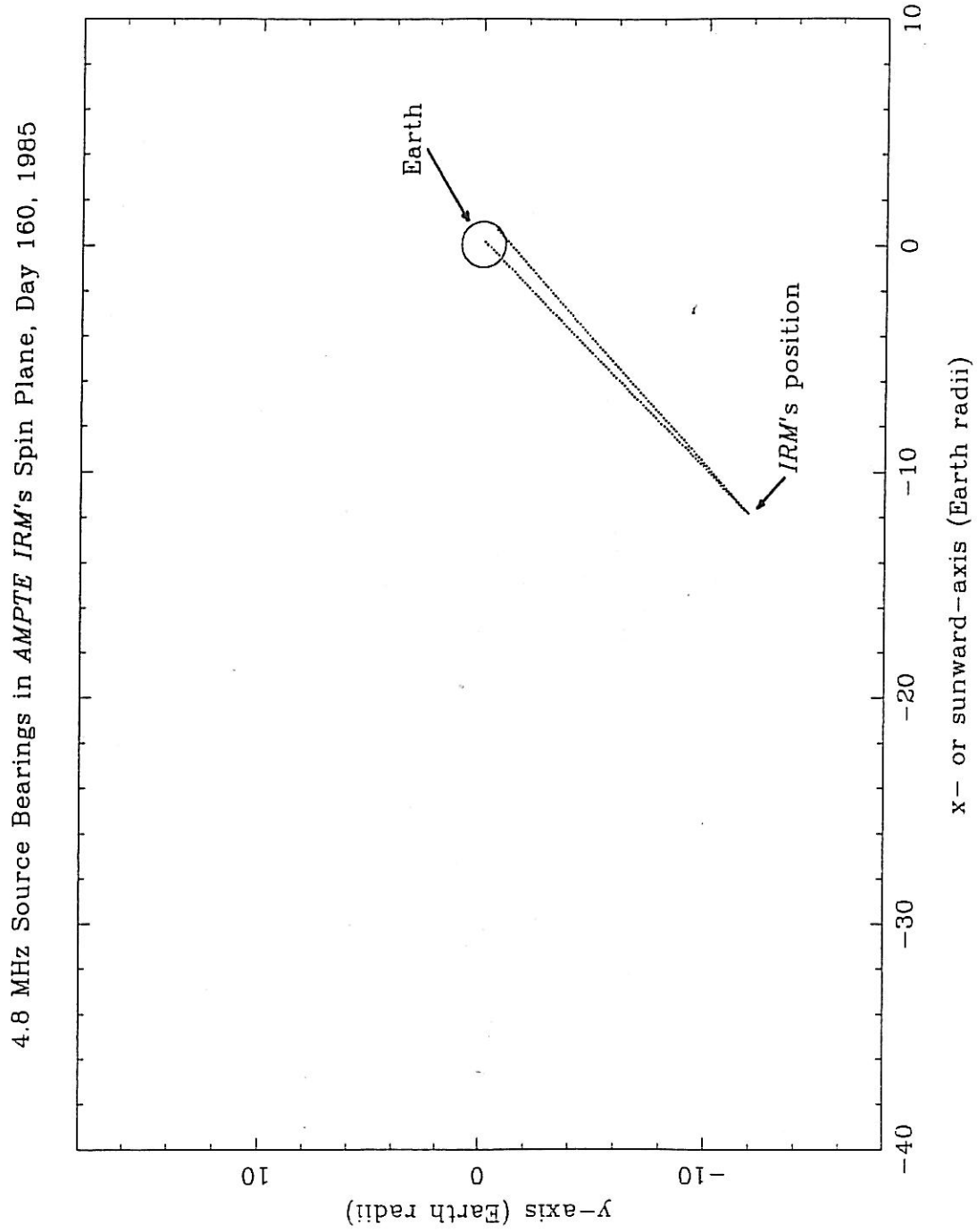
4.8 MHz Source Bearings in AMPTE IRM's Spin Plane, Day 160, 1985
Earth
IRM's position
y-axis (Earth radii)
x- or sunward-axis (Earth radii)
10
0
-10
10
0
-10
-20
-30
-40

Figure 18. Direction of the source of the spin-correlated 4.8 MHz data in the *IRM*'s spin plane on 4-5 March 1986. The projection of the Earth in this plane is denoted by the circle drawn, the projection of the spacecraft's course is the jagged line indicated, and the source directions are the dotted lines running between them.

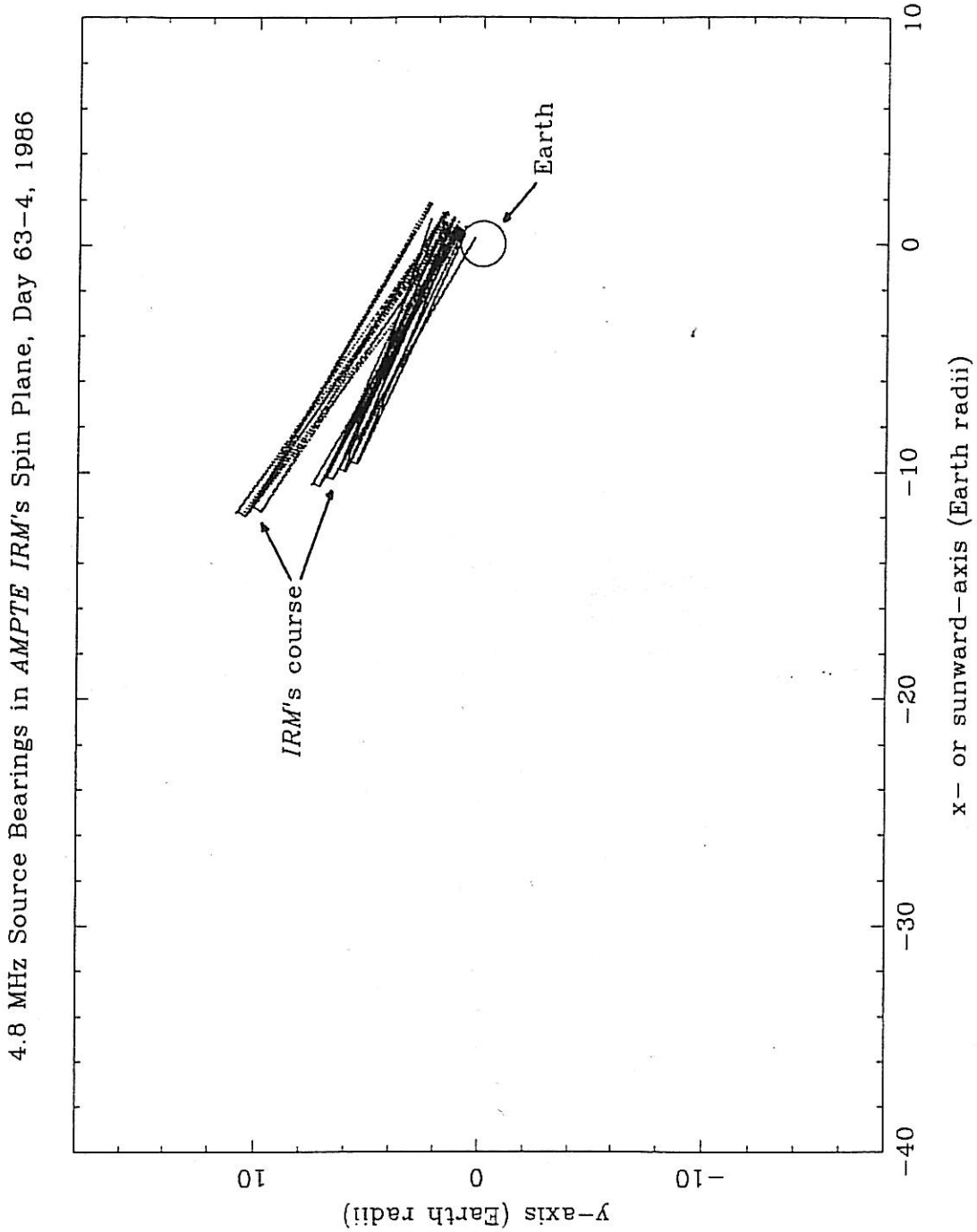
4.8 MHz Source Bearings in AMPTE IRM's Spin Plane, Day 63-4, 1986
IRM's course
Earth
y-axis (Earth radii)
x- or sunward-axis (Earth radii)
10
0
-10
10
0
-10
-20
-30
-40

Figure 19. Direction of the source of the 454 and 504 kHz Auroral Kilometric Radiation data in the *IRM*'s spin plane on 27 December 1984. The projection of the Earth in this plane is denoted by the circle drawn, the projection of the spacecraft's course is the jagged line indicated, and the source directions are the dotted lines running between them.

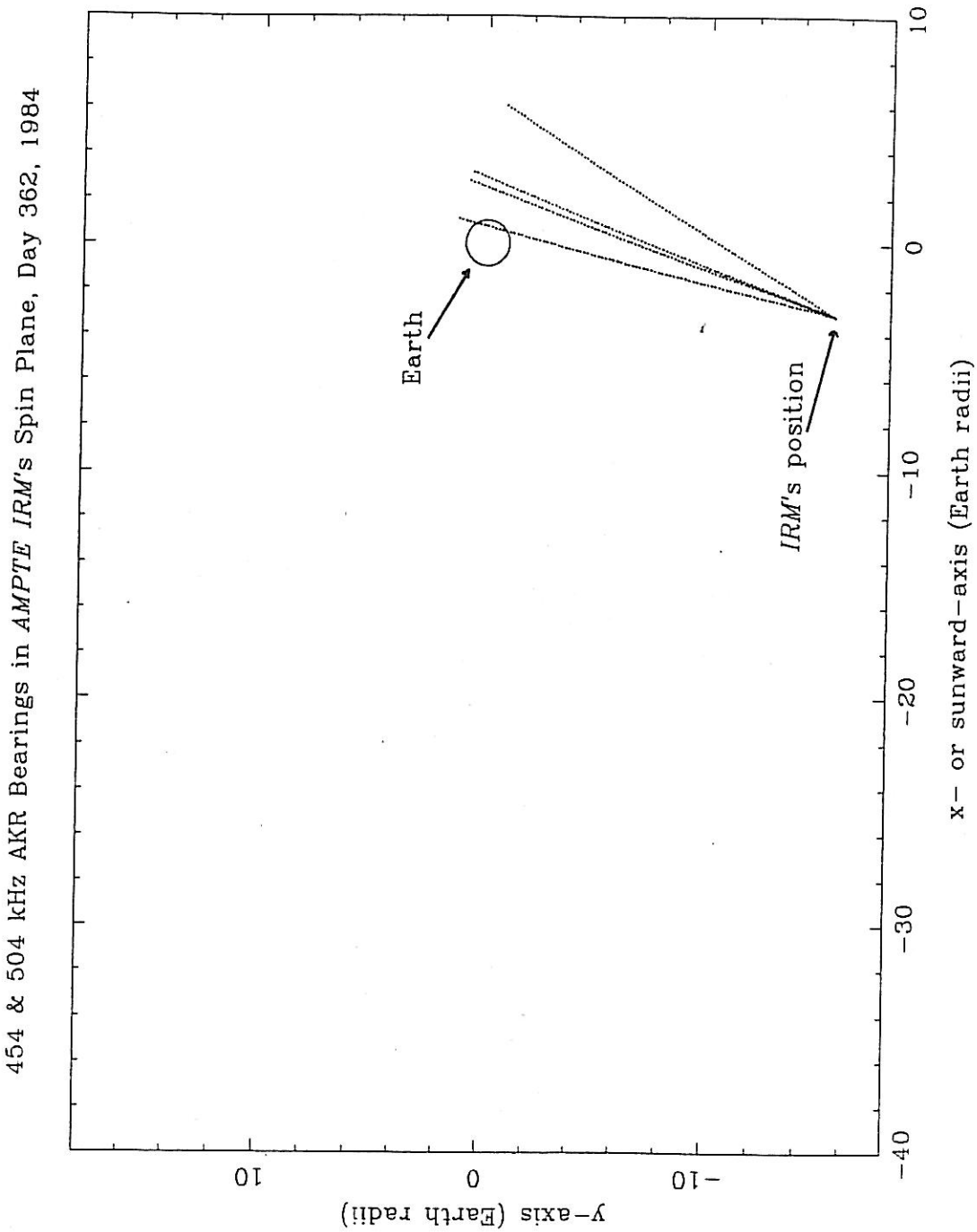
454 & 504 kHz AKR Bearings in AMPTE IRM's Spin Plane, Day 362, 1984
Earth
IRM's position
y-axis (Earth radii)
x- or sunward-axis (Earth radii)
10
0
-10
-40
-30
-20
-10
0
10

Figure 20. Direction of the source of the 302 kHz Auroral Kilometric Radiation data in the *IRM*'s spin plane on 4 March 1986. The projection of the Earth in this plane is denoted by the circle drawn, the projection of the spacecraft's course is the jagged line indicated, and the source directions are the dotted lines running between them.

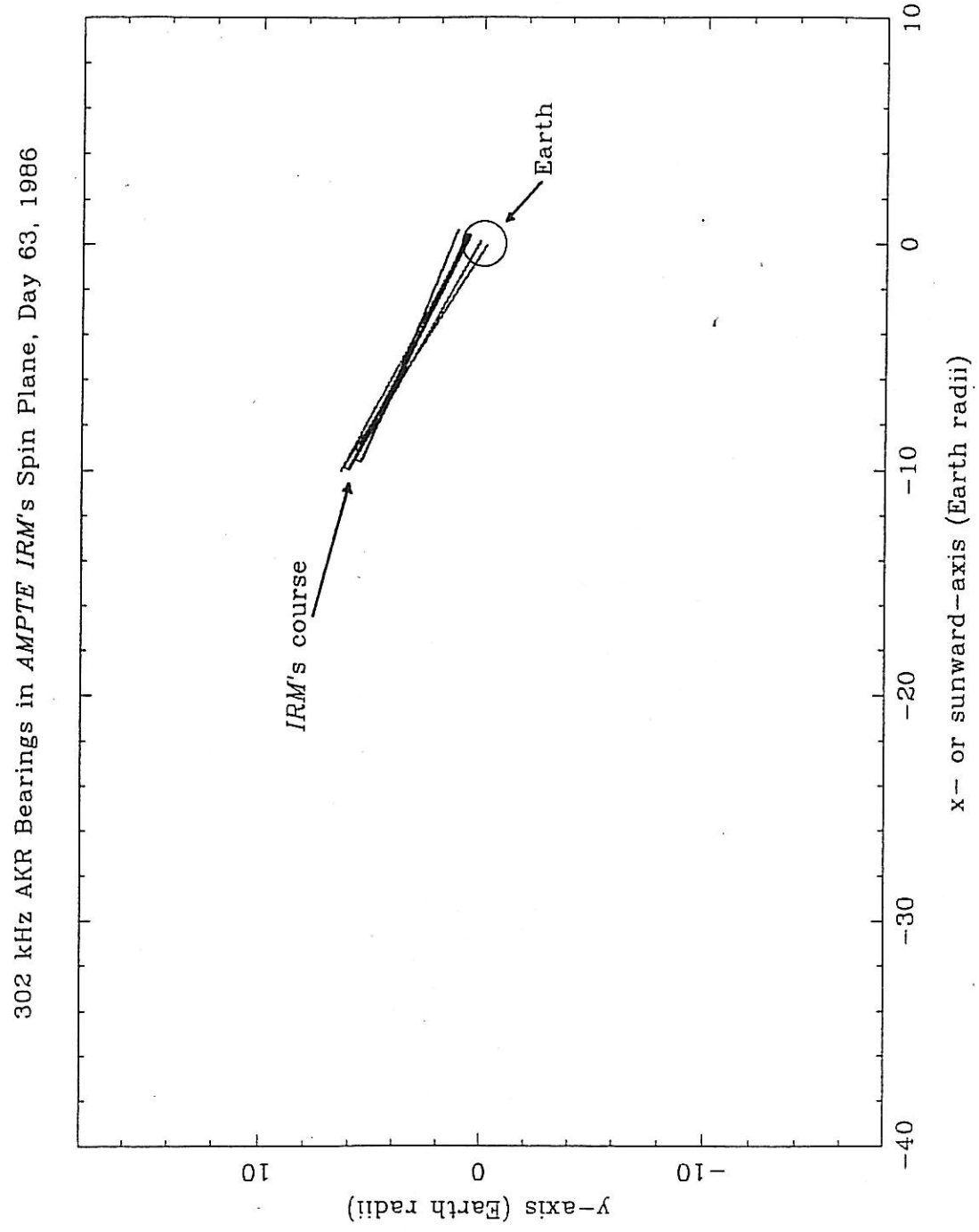
302 kHz AKR Bearings in AMPTE IRM's Spin Plane, Day 63, 1986
IRM's course
Earth
y-axis (Earth radii)
x- or sunward-axis (Earth radii)
10
0
-10
10
0
-10
-20
-30
-40

Figure 21. Graphic display of possible source directions. The plane of the page is the source plane: perpendicular to the spin plane and along the Φ direction. Θ, the out-of-spin-plane source angle, determines the four rays a free source may lie along, indicated by the circled points. Presence of background noise implies the arc between the points on one side of the spin axis or the other. Triangulation determines which pair of points is meaningful.

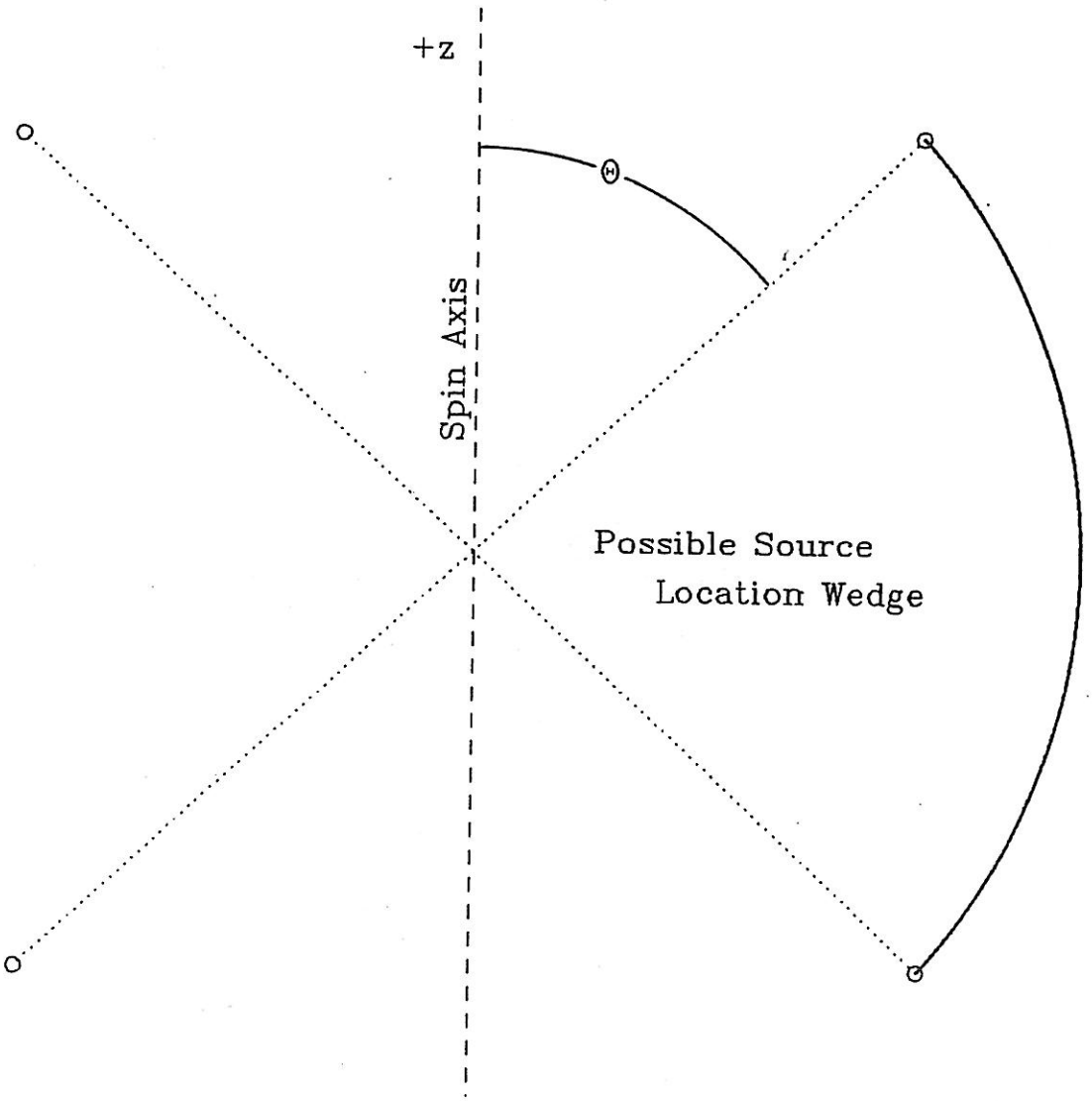
+z
Spin Axis
Possible Source
Location Wedge

Figure 22. This set of 3 plots display the source arcs of the 4.8 MHz signal as seen from the *IRM* on 27 December 1984. The Earth, as seen from the spacecraft, is the circle and is scaled to its apparent size; the Sun's position is indicated by the point labelled; and the source positions are the vertical segments. This figure indicates a source somewhat in front of the Earth.

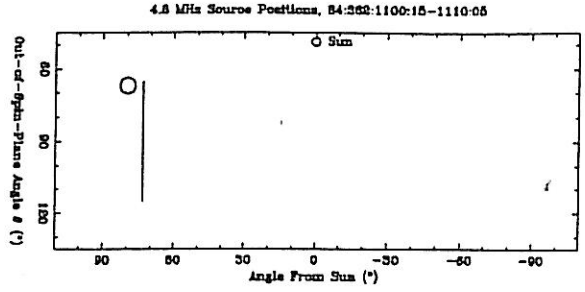
4.8 MHz Source Positions, 84:362:1100:15-1110:05
Sun
Out-of-Ecpln-Plane Angle ϕ (°)
60
90
120
90
60
30
0
-30
-60
-90
Angle From Sun (°)

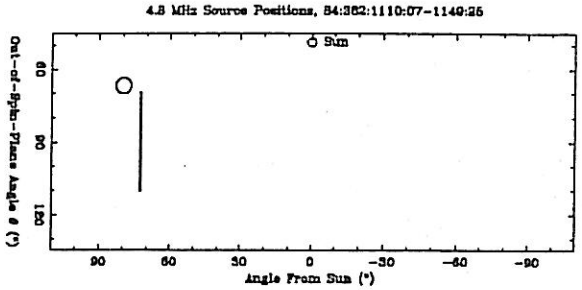
4.8 MHz Source Positions, 84:362:1110:07-1149:25
Sun
Out-of-Ecpln-Plane Angle ϕ (°)
60
90
120
90
60
30
0
-30
-60
-90
Angle From Sun (°)

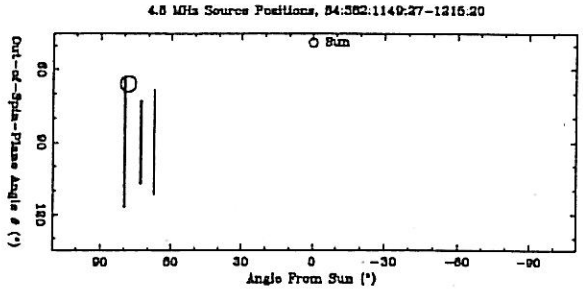
4.8 MHz Source Positions, 84:362:1149:27-1215:20
Sun
Out-of-Ecpln-Plane Angle ϕ (°)
60
90
120
90
60
30
0
-30
-60
-90
Angle From Sun (°)

Figure 23. This set of 4 plots display the source arcs of the 4.8 MHz signal as seen from the *IRM* on 21 April 1985. The Earth, as seen from the spacecraft, is the circle and is scaled to its apparent size; the Sun's position is indicated by the point labelled; and the source positions are the vertical segments. This figure indicates a source somewhere on the Earth.

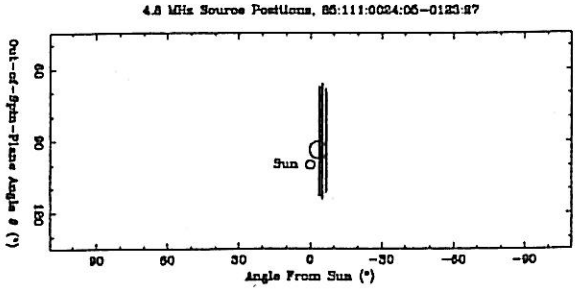
4.8 MHz Source Positions, 86:111:0024:05-0123:27
Out-of-Ecliptic-Plane Angle φ (°)
Sun
Angle From Sun (°)

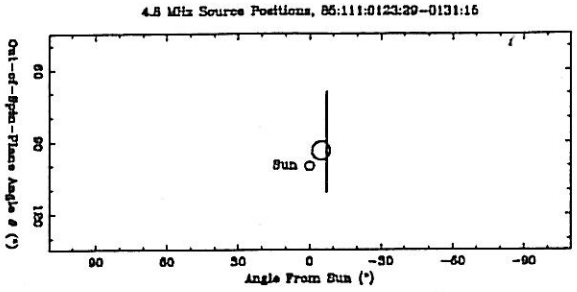
4.8 MHz Source Positions, 86:111:0123:29-0131:16
Out-of-Ecliptic-Plane Angle φ (°)
Sun
Angle From Sun (°)

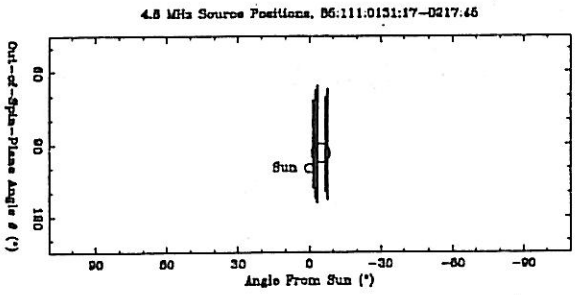
4.8 MHz Source Positions, 86:111:0131:17-0217:46
Out-of-Ecliptic-Plane Angle φ (°)
Sun
Angle From Sun (°)

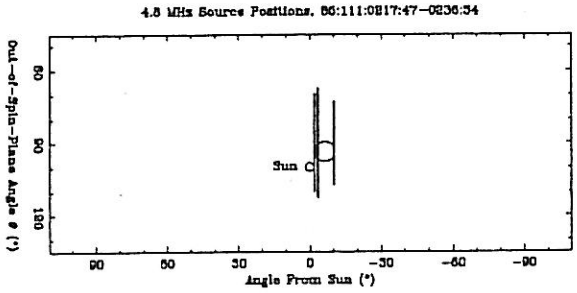
4.8 MHz Source Positions, 86:111:0217:47-0236:34
Out-of-Ecliptic-Plane Angle φ (°)
Sun
Angle From Sun (°)

Figure 24. This set of 5 plots display the source arcs of the 4.8 MHz signal as seen from the *IRM* on 8 June 1985. The Earth, as seen from the spacecraft, is the circle and is scaled to its apparent size; the Sun's position is indicated by the point labelled; and the source positions are the vertical segments. This figure indicates a source somewhere on the Earth.

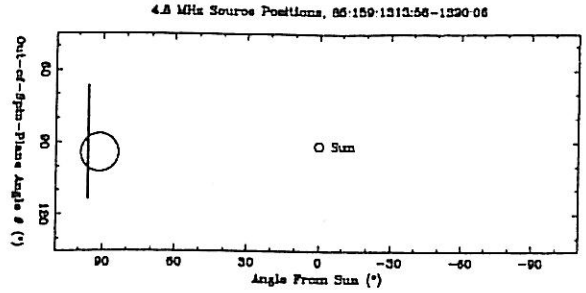
4.8 MHz Source Positions, 86:159:1313:58-1330:06
Out-of-Spin-Plane Angle φ (°)
60
90
120
O Sun
90
60
30
0
-30
-60
-90
Angle From Sun (°)

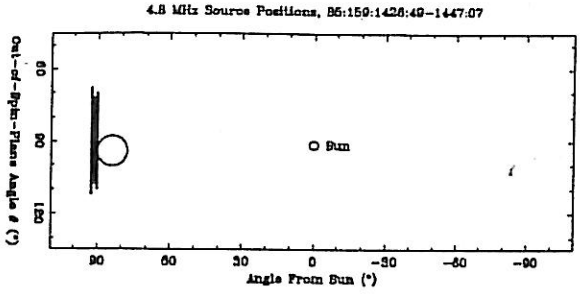
4.8 MHz Source Positions, 86:159:1426:49-1447:07
Out-of-Spin-Plane Angle φ (°)
60
90
120
O Sun
90
60
30
0
-30
-60
-90
Angle From Sun (°)

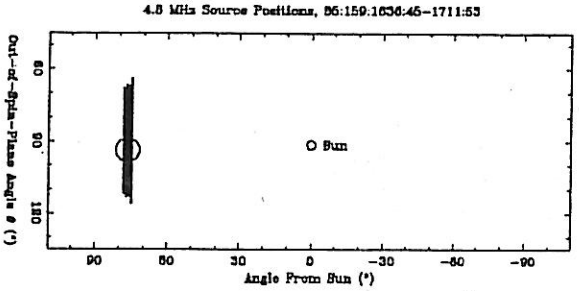
4.8 MHz Source Positions, 86:159:1636:45-1711:53
Out-of-Spin-Plane Angle φ (°)
60
90
120
O Sun
90
60
30
0
-30
-60
-90
Angle From Sun (°)

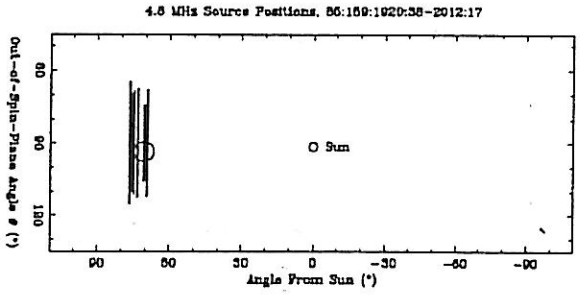
4.8 MHz Source Positions, 86:159:1920:38-2012:17
Out-of-Spin-Plane Angle φ (°)
60
90
120
O Sun
90
60
30
0
-30
-60
-90
Angle From Sun (°)

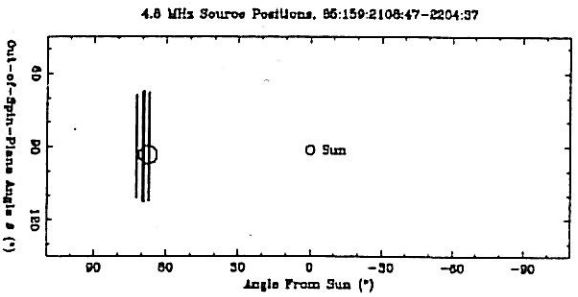
4.8 MHz Source Positions, 86:159:2108:47-2204:37
Out-of-Spin-Plane Angle φ (°)
60
90
120
O Sun
90
60
30
0
-30
-60
-90
Angle From Sun (°)

Figure 25. This plot displays the source arcs of the 4.8 MHz signal as seen from the *IRM* on 9 June 1985. The Earth, as seen from the spacecraft, is the circle and is scaled to its apparent size; the Sun's position is indicated by the point labelled; and the source positions are the vertical segments. This figure a indicates source somewhere on the Earth.

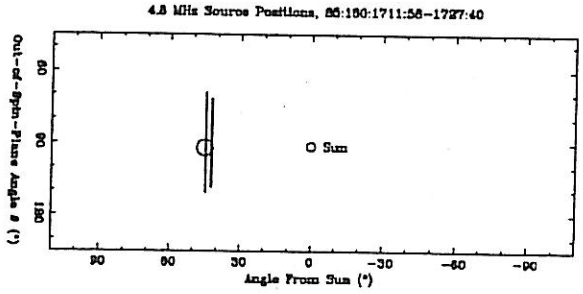
4.8 MHz Source Positions, 85:160:1711:58-1727:40
Out-of-Sph-Plane Angle θ (°)
60
90
180
Sun
90
60
30
0
-30
-60
-90
Angle From Sun (°)

Figure 26. This set of 5 plots display the source arcs of the 4.8 MHz signal as seen from the *IRM* on 4-5 March 1986. The Earth, as seen from the spacecraft, is the circle and is scaled to its apparent size; the Sun's position is indicated by the point labelled; and the source positions are the vertical segments. This figure indicates a source somewhat in front of the Earth.

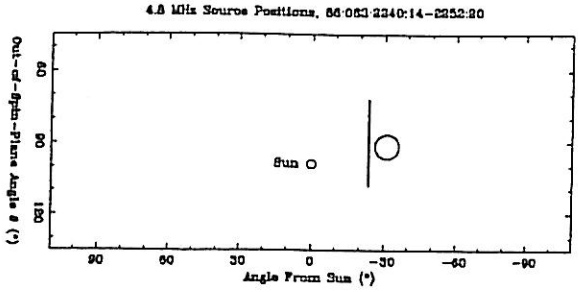
4.8 MHz Source Positions, 86:063:2340:14-2352:20
Out-of-Spin-Plane Angle θ (°)
60
90
120
Sun
90
60
30
0
-30
-60
-90
Angle From Sun (°)

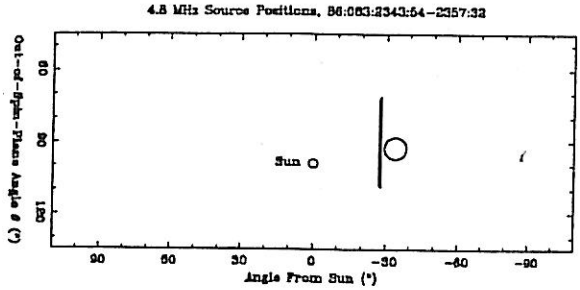
4.8 MHz Source Positions, 86:063:2343:54-2357:32
Out-of-Spin-Plane Angle θ (°)
60
90
120
Sun
90
60
30
0
-30
-60
-90
Angle From Sun (°)

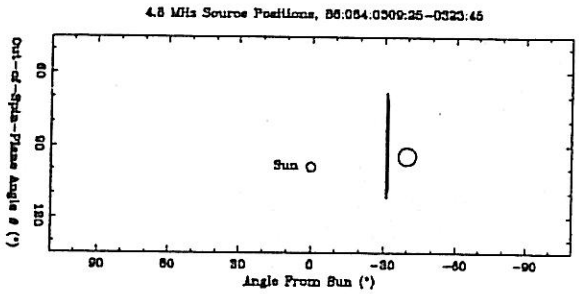
4.8 MHz Source Positions, 86:064:0309:25-0323:45
Out-of-Spin-Plane Angle θ (°)
60
90
120
Sun
90
60
30
0
-30
-60
-90
Angle From Sun (°)

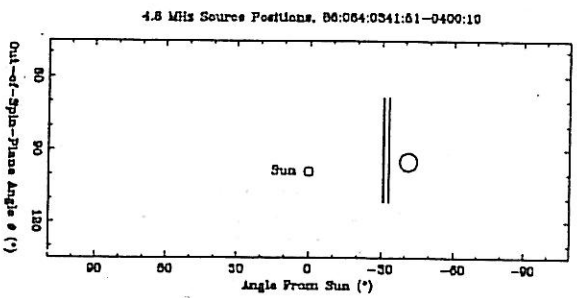
4.8 MHz Source Positions, 86:064:0341:51-0400:10
Out-of-Spin-Plane Angle θ (°)
60
90
120
Sun
90
60
30
0
-30
-60
-90
Angle From Sun (°)

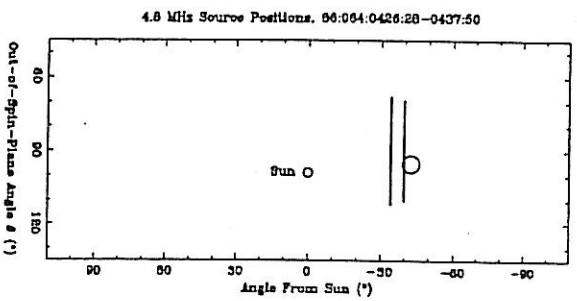
4.8 MHz Source Positions, 86:064:0426:28-0437:50
Out-of-Spin-Plane Angle θ (°)
60
90
120
Sun
90
60
30
0
-30
-60
-90
Angle From Sun (°)

Figure 27. This set of 2 plots display the source arcs of the 454 and 504 kHz AKR as seen from the *IRM* on 27 December 1984. The Earth, as seen from the spacecraft, is the circle and is scaled to its apparent size; the Sun's position is indicated by the point labelled; and the source positions are the vertical segments. This figure indicates a source somewhat in front of the Earth, just like the 4.8 MHz signal.

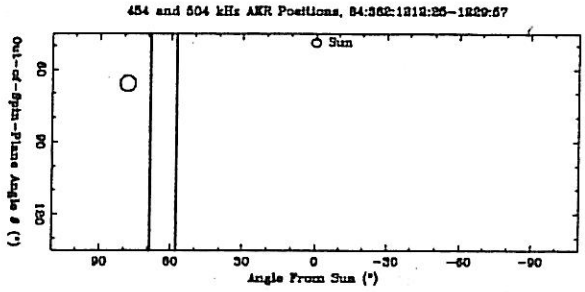
454 and 504 kHz AKR Positions, 84:362:1212:26–1229:57
Sun
Out-of-Ecliptic-Plane Angle φ (°)
60
90
120
90
60
30
0
-30
-60
-90
Angle From Sun (°)

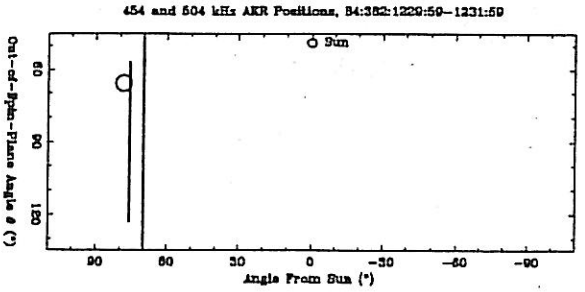
454 and 504 kHz AKR Positions, 84:362:1229:59–1231:59
Sun
Out-of-Ecliptic-Plane Angle φ (°)
60
90
120
90
60
30
0
-30
-60
-90
Angle From Sun (°)

Figure 28. This set of 5 plots display the source arcs of the 302 kHz AKR as seen from the *IRM* on 4 March 1986. The Earth, as seen from the spacecraft, is the circle and is scaled to its apparent size; the Sun's position is indicated by the point labelled; and the source positions are the vertical segments. This figure indicates a source somewhere near the Earth.

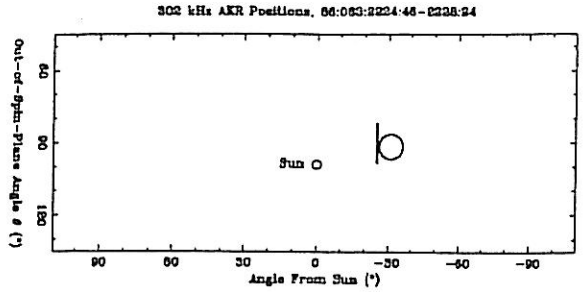
302 kHz AKR Positions, 86:063:2224:46-2228:24
Out-of-Spin-Plane Angle θ (°)
60
90
120
Sun
90
60
30
0
-30
-60
-90
Angle From Sun (°)

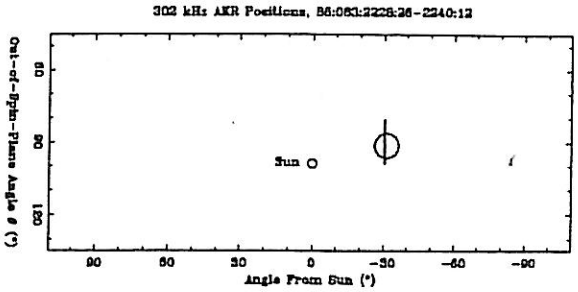
302 kHz AKR Positions, 86:063:2228:36-2240:12
Out-of-Spin-Plane Angle θ (°)
60
90
120
Sun
90
60
30
0
-30
-60
-90
Angle From Sun (°)

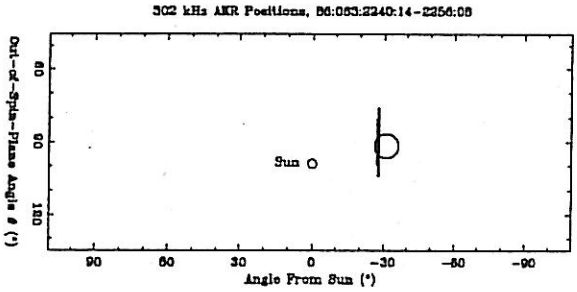
302 kHz AKR Positions, 86:063:2240:14-2256:08
Out-of-Spin-Plane Angle θ (°)
60
90
120
Sun
90
60
30
0
-30
-60
-90
Angle From Sun (°)

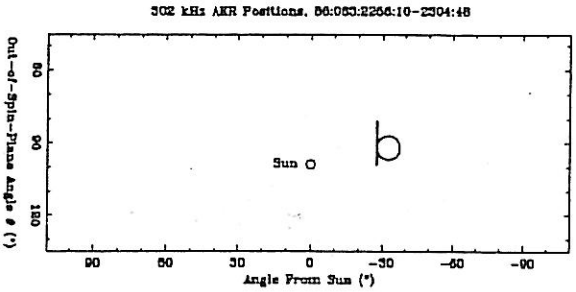
302 kHz AKR Positions, 86:063:2256:10-2304:48
Out-of-Spin-Plane Angle θ (°)
60
90
120
Sun
90
60
30
0
-30
-60
-90
Angle From Sun (°)

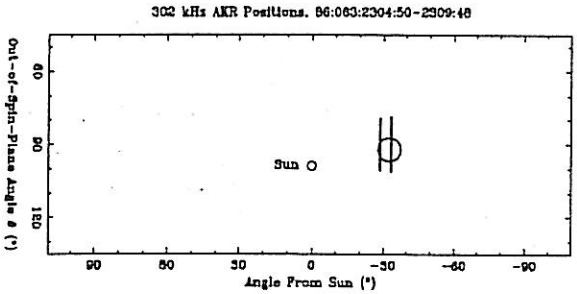
302 kHz AKR Positions, 86:063:2304:50-2309:48
Out-of-Spin-Plane Angle θ (°)
60
90
120
Sun
90
60
30
0
-30
-60
-90
Angle From Sun (°)

Figure 29. Graph of calculated electric field strength versus distance from the Earth for all measurements taken, with error bars. A least-squares fit has been applied, and the resulting slope and correlation coefficient noted (a coefficient of 1.0 means a perfect fit).

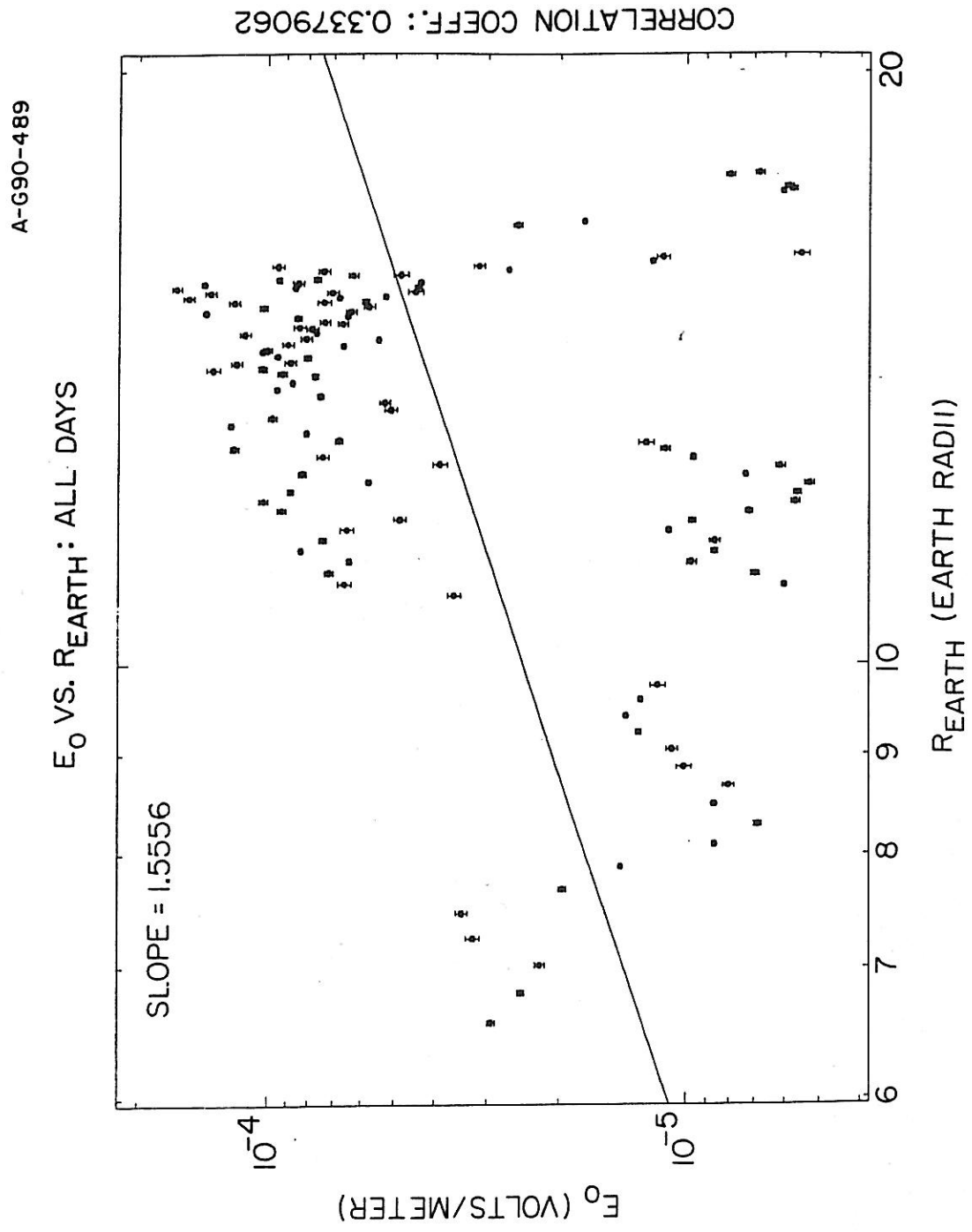
A-690-489
E_o VS. R_{EARTH}: ALL DAYS
CORRELATION COEFF.: 0.3379062
SLOPE = 1.5556
E_o (VOLTS/METER)
10^{-4}
10^{-5}
6
7
8
9
10
20
R_{EARTH} (EARTH RADII)

Figure 30. Graph of calculated electric field strength versus distance from the Earth for each separate continuous receiving period, with error bars. A least-squares fit has been applied to each, and the resulting slope and correlation coefficient noted (a coefficient of 1.0 means a perfect fit).

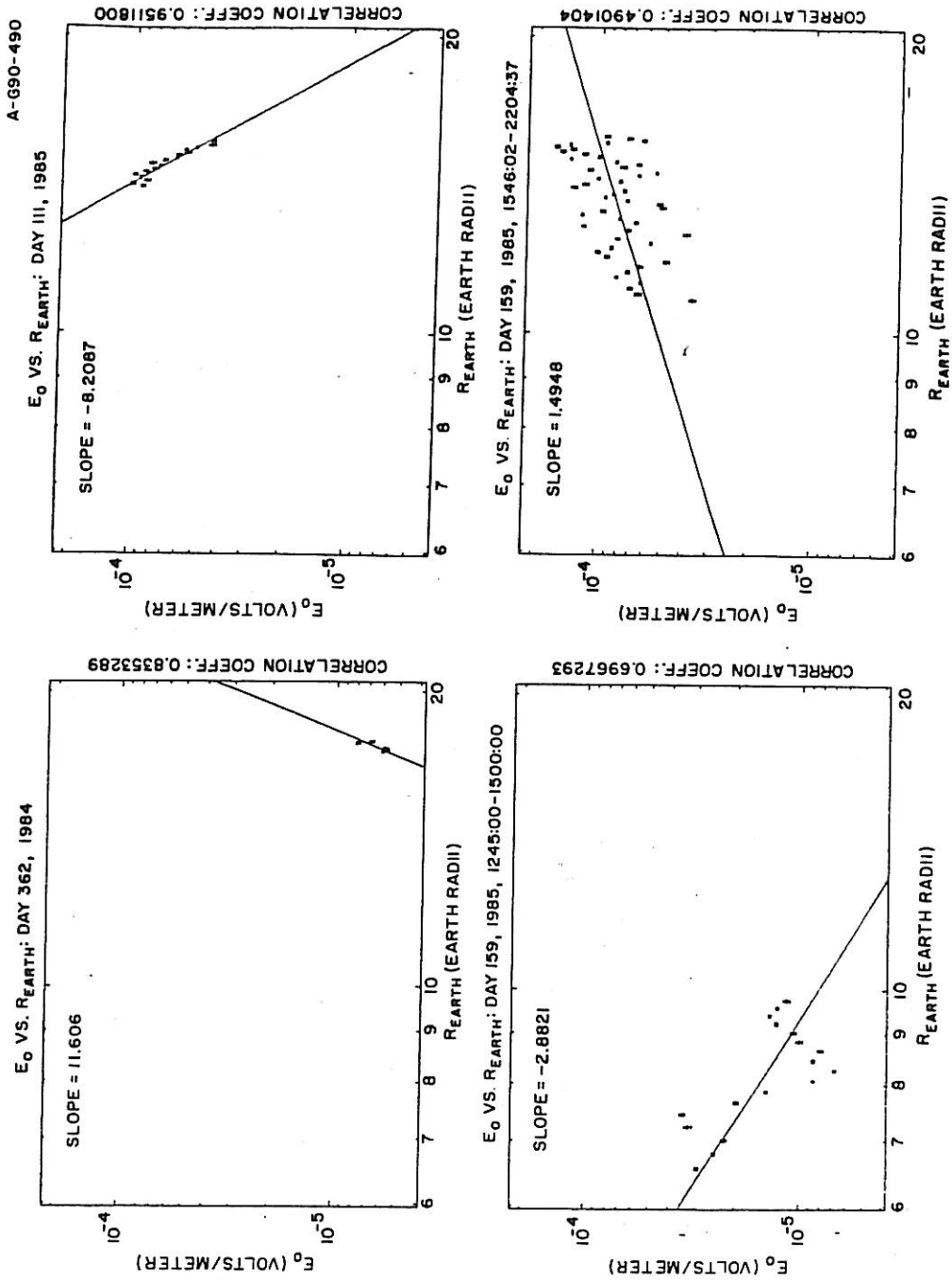
A-690-490
E_o VS. R_{EARTH}: DAY 111, 1985
SLOPE = -8.2087
CORRELATION COEFF.: 0.9511800
E_o VS. R_{EARTH}: DAY 159, 1985, 1546:02-2204:37
SLOPE = 1.4948
CORRELATION COEFF.: 0.4901404
E_o VS. R_{EARTH}: DAY 362, 1984
SLOPE = 11.606
CORRELATION COEFF.: 0.8353289
E_o VS. R_{EARTH}: DAY 159, 1985, 1245:00-1500:00
SLOPE = -2.8821
CORRELATION COEFF.: 0.6967293
E_o (VOLTS/METER)
R_{EARTH} (EARTH RADII)

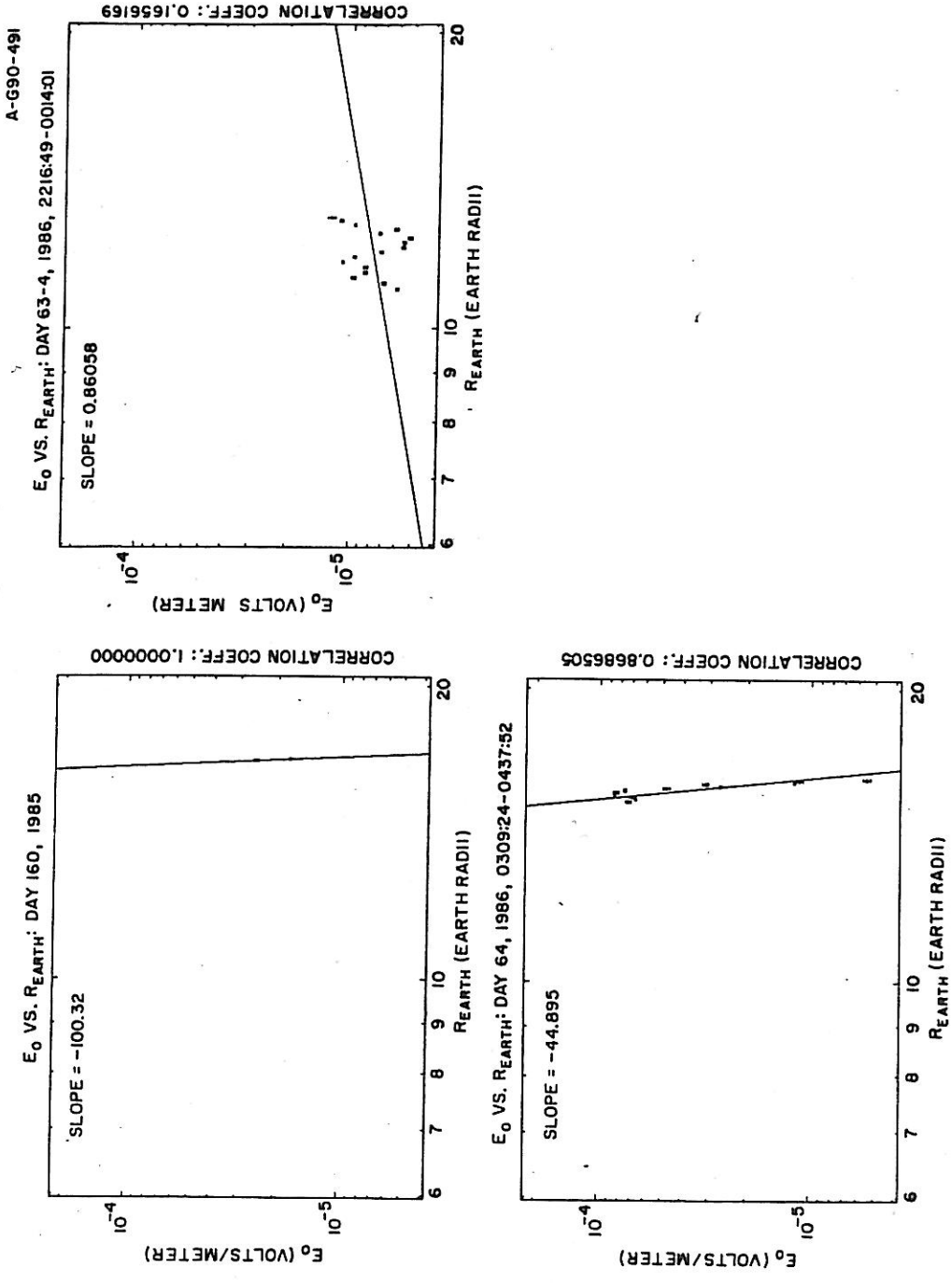

Figure 30 — continued